SANDIA REPORT

SAND95–2081 • UC–814
Unlimited Release
Printed January 1996

Yucca Mountain Site Characterization Project

Solution of Problems with Material Nonlinearities with a Coupled Finite Element/Boundary Element Scheme Using an Iterative Solver

J. Richard Koteras

Prepared by
Sandia National Laboratories
Albuquerque, New Mexico 87185 and Livermore, California 94550
for the United States Department of Energy
under Contract DE-AC04-94AL85000

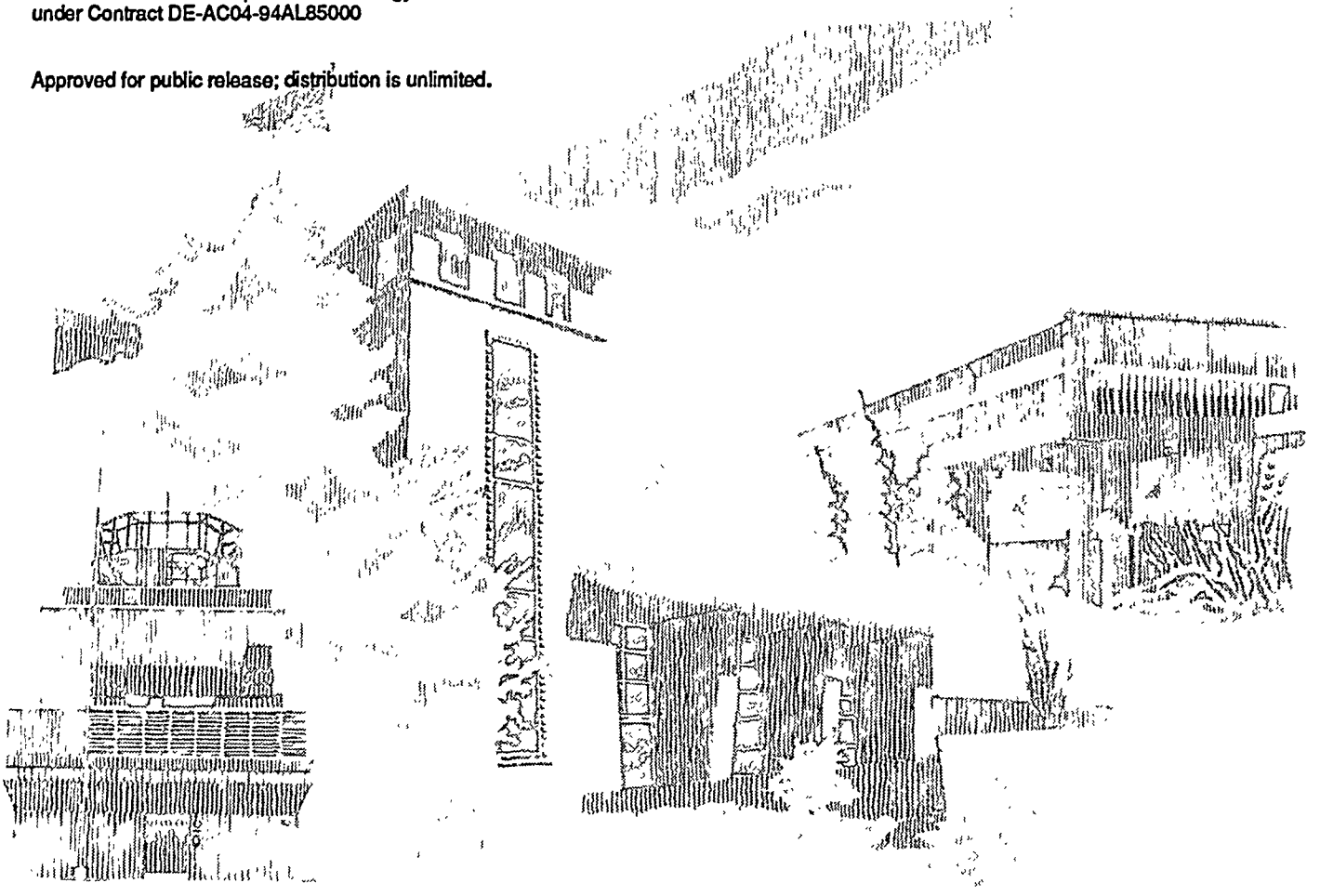

SF2900Q(8-81)

"Prepared by Yucca Mountain Site Characterization Project (YMSCP) participants as part of the Civilian Radioactive Waste Management Program (CRWM). The YMSCP is managed by the Yucca Mountain Project Office of the U.S. Department of Energy, DOE Field Office, Nevada (DOE/NV). YMSCP work is sponsored by the Office of Geologic Repositories (OGR) of the DOE Office of Civilian Radioactive Waste Management (OCRWM)."

Issued by Sandia National Laboratories, operated for the United States Department of Energy by Sandia Corporation.

Available to DOE and DOE contractors from
Office of Scientific and Technical Information
PO Box 62
Oak Ridge, TN 37831

Prices available from (615) 576-8401, FTS 626-8401

Available to the public from
National Technical Information Service
US Department of Commerce
5285 Port Royal Rd
Springfield, VA 22161

NTIS price codes
Printed copy: A03
Microfiche copy: A01

SAND95-2081
Unlimited Release
Printed January 1996

Distribution
Category UC-814

Solution of Problems with Material Nonlinearities with a Coupled Finite Element/Boundary Element Scheme Using an Iterative Solver

J. Richard Koteras
Engineering and Manufacturing Mechanics Department
Sandia National Laboratories
Albuquerque, NM 87185

Abstract

The prediction of stresses and displacements around tunnels buried deep within the earth is an important class of geomechanics problems. The material behavior immediately surrounding the tunnel is typically nonlinear. The surrounding mass, even if it is nonlinear, can usually be characterized by a simple linear elastic model. The finite element method is best suited for modeling nonlinear materials of limited volume, while the boundary element method is well suited for modeling large volumes of linear elastic material. A computational scheme that couples the finite element and boundary element methods would seem particularly useful for geomechanics problems. A variety of coupling schemes have been proposed, but they rely on direct solution methods. Direct solution techniques have large storage requirements that become cumbersome for large-scale three-dimensional problems. An alternative to direct solution methods is iterative solution techniques. A scheme has been developed for coupling the finite element and boundary element methods that uses an iterative solution method. This report shows that this coupling scheme is valid for problems where nonlinear material behavior occurs in the finite element region.

Contents

Solution of Problems with Material Nonlinearities with a Coupled Finite Element/Boundary Element Scheme Using an Iterative Solver

Figures

This work was conducted at Sandia National Laboratories for the U. S. Department of Energy under Contract No. DE-AC04-94AL85000. This work activity was directed and planned using Work Agreement WA-0070, Revision 00, for work description WBS 1.2.4.2.3.1 for the Yucca Mountain Site Characterization Project.

Solution of Problems with Material Nonlinearities with a Coupled Finite Element/Boundary Element Scheme Using an Iterative Solver

Introduction

An important class of geomechanics problems involves tunnels buried deep within the earth. The material behavior immediately surrounding the tunnel is typically nonlinear and can exhibit behavior such as plastic deformation, slip on joint planes, or creep. The surrounding mass can also be nonlinear, but its overall effect can usually be captured by using a simple linear elastic material model. When these problems are studied with computer models, it is desirable to have a model that captures the nonlinear effects in the material adjacent to the tunnels and to model a large volume of surrounding material.

The finite element method is well suited for modeling regions with rapidly varying properties and nonlinear material behavior. It is an expensive computational tool when trying to model large volumes. The boundary element method, on the other hand, offers a means to model large volumes of material efficiently because only the boundary of the volume needs to be discretized. If material properties vary significantly over a portion of the domain or if the material behaves nonlinearly, then use of the boundary element approach becomes cumbersome relative to the finite element method. The boundary element model is best suited, therefore, for large regions of linear elastic material or large regions whose overall influence can be captured by a linear elastic material behavior.

A computational scheme that couples the finite element and boundary element methods would seem well suited for geomechanics problems. A variety of coupling schemes have been proposed, but they rely on direct solution methods[1-8]. Direct solution techniques have large storage requirements and become cumbersome for large-scale problems. An alternative to direct solution methods is iterative solution techniques. Iterative solution methods eliminate the problem of large storage requirements and can be more efficient solvers for large three-dimensional problems than direct solutions techniques. A scheme has been developed for coupling the finite element and boundary element methods that uses an iterative solution technique. The use of an iterative solution technique means that the coupling scheme can be applied to large-scale models such as those that would be encountered in three-dimensional geomechanics problems. It has been shown that the coupling scheme is valid for purely elastic problems[9]. This report presents results from problems showing that the coupling scheme is also valid when nonlinear material behavior occurs in the finite element portion of the model.

The main purpose of this report is, therefore, to establish the validity and accuracy of a coupled finite element/boundary element using an iterative solution technique for a class of problems where there is nonlinear material behavior in the finite element region. The iterative solution technique uses a Newton scheme to set up a system of linear equations for a load step. The system of equations is solved by using a conjugate gradient method for nonsymmetric operators since the coupling scheme leads to nonsymmetric matrices. This scheme has been implemented in the JAC2D[10] finite element code. A more detailed discussion of this solution approach is given in following sections of the report. For the initial work involving only elastic materials, it was not necessary to use an incremental loading approach. A solution scheme based solely on the conjugate gradient method for nonsymmetric operators was sufficient for solving this class of problems. The extension of the coupled finite element/boundary element method to problems involving nonlinear material behavior required a different solution strategy.

The problems in this report are two-dimensional problems only. In the concluding remarks, comments will be made about the extension of this work to three dimensions and efficiency considerations for such an implementation.

This report presents a number of problems where a region with nonlinear material behavior is surrounded by a linear elastic region. Two different nonlinear material models are used, an elastic-plastic model and a jointed rock model.

Elastic-Plastic Problems

The first nonlinear material model used in the coupled scheme is an elastic-plastic material model. This material model is used in conjunction with the problem of a pressurized cylindrical cavity in an infinite medium. The accuracy of numerical results for this problem can be assessed by studying results for an analytic solution for the elastic-plastic state of a thick-walled tube. The first part of this report presents key results from the analytic solution. Results are then presented from numerical studies of a pressurized cylindrical cavity in an infinite region for cases where the pressure becomes large enough to generate plastic deformation in the area around the cavity.

Elastic-Plastic State of a Thick-Walled Tube

The geometry for the thick-walled tube is shown in Figure 1. The tube has an inner radius, a, and an outer radius, b. The internal pressure is p. The problem of determining analytic expressions for the displacements and stresses for the tube in an elastic-perfectly plastic state is discussed in Reference 11. It is not possible to obtain an exact analytic solution for this problem. As Reference 11 points out, however, "it is possible to obtain a simple approximate solution if we introduce a number of simplifications, which are justified by the results of numerical integration." The full details of the derivation of an approximate solution will not be presented as the derivation is quite lengthy. Only key results from the solution in Reference 11 are presented. The accuracy of the solution in Reference 11 will

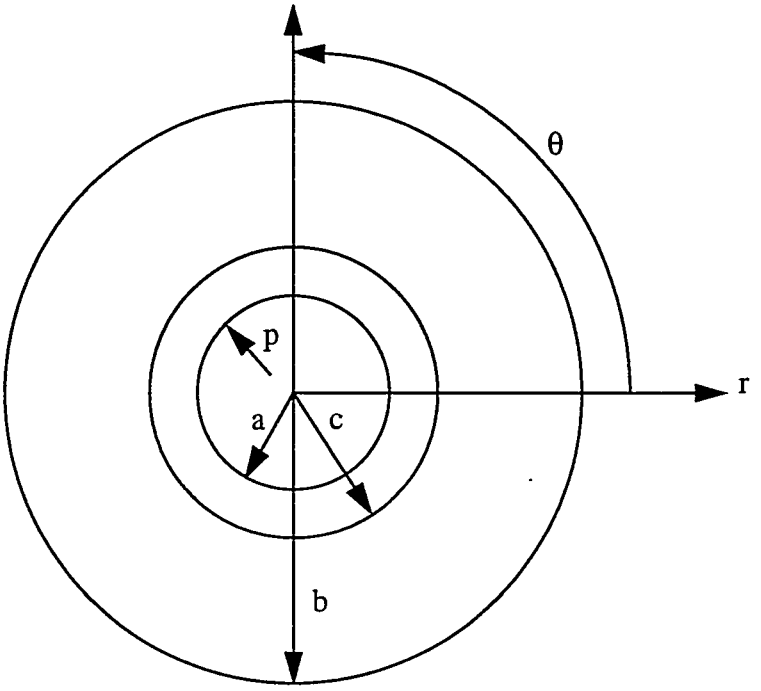

Figure 1. Cylindrical Tube Under Pressure

be discussed in later sections when numerical results are presented for the problem of a pressurized tube. The analytic solution for this problem is presented in terms of a cylindrical coordinate system, $r\theta z$. The origin of the cylindrical coordinate system coincides with the center of the cavity, and the z axis runs the length of the cylindrical cavity. The solution is for the plane strain case.

When the tube is completely elastic, the radial and tangential stresses, σ_r and σ_θ, are given by the well know Lame' solution

$$\sigma_r = -p'(b^2/r^2 - 1), \qquad \text{(EQ 1)}$$

$$\sigma_\theta = p'(b^2/r^2 + 1), \qquad \text{(EQ 2)}$$

where

$$p' = pa^2/(b^2 - a^2). \qquad \text{(EQ 3)}$$

The axial stress component, σ_z, for the general case (compressible material) is given by

$$\sigma_z = \nu(\sigma_r + \sigma_\theta), \qquad \text{(EQ 4)}$$

where ν is Poisson's ratio. For the incompressible case ($\nu = 0.5$), the axial stress is

$$\sigma_z = p' = (\sigma_r + \sigma_\theta)/2. \quad \text{(EQ 5)}$$

The radial displacement u_r for the general case (compressible material) is given by

$$u_r = \frac{[(1+\nu)b^2/r + (1-\nu-2\nu^2)r]pa^2}{E(b^2-a^2)}, \quad \text{(EQ 6)}$$

where E is the modulus of elasticity. For the incompressible case, the radial displacement is given by

$$u_r = 3pa^2b^2/[2Er(b^2-a^2)]. \quad \text{(EQ 7)}$$

When p becomes large enough to yield the material, an interface between the plastic and elastic zones is a circle with radius c. The location of the interface is a function of the geometry of the tube, the internal pressure, p, and the yield stress in shear, τ_s. The radius c for the plastic zone is given by

$$p/(2\tau_s) = (1-c^2/b^2)/2 + \ln(c/a). \quad \text{(EQ 8)}$$

The radial and tangential stresses in the plastic zone ($a \le r \le c$) are given by

$$\sigma_r = -p + 2\tau_s \ln(r/a) \quad \text{(EQ 9)}$$

and

$$\sigma_\theta = -p + 2\tau_s[1 + \ln(r/a)]. \quad \text{(EQ 10)}$$

The radial displacement in the plastic zone is given by

$$u_r = (\tau_s c^2)/(Er). \quad \text{(EQ 11)}$$

The radial and tangential stresses in the elastic zone ($c < r < b$) are given by Equations (1) and (2) if q' is substituted for p', where q' is defined as

$$q' = -qc^2/(b^2-c^2). \quad \text{(EQ 12)}$$

In Equation (12), q is the radial stress on the interface line $r = c$.

A special case of the above problem that is of interest in the study of a circular cavity in an infinite medium (the problem to be studied with the coupled finite element/boundary element technique) is the case where $b \gg a$ and $b \gg c$. If $b \gg a$ and $b \gg c$, then Equation (8) can be rewritten as

$$p/(2\tau_s) \approx 1/2 + \ln(c/a). \quad \text{(EQ 13)}$$

Equation (13) can be rewritten as

$$p = 2\tau_s[1/2 + \ln(c/a)] \qquad \text{(EQ 14)}$$

so that p is simply a function of c. Equation (13) can be used to solve directly for c. The value for c is given by

$$c = a\exp[p/(2\tau_s) - 1/2]. \qquad \text{(EQ 15)}$$

Once a value for c is determined by using Equation (15), it is possible to easily calculate the value for the radial displacement at the inner boundary ($r = a$) by using Equation (11). At the inner boundary,

$$u_r = (\tau_s c^2)/(Ea) \qquad \text{(EQ 16)}$$

after yielding has occurred at the inner boundary. Equations (15) and (16) are particularly useful in the study of the problem of a pressurized cylindrical cavity in an infinite medium with numerical techniques. In subsequent sections, the preceding analytic solutions for the elastic-plastic behavior of a pressurized tube (pressurized cavity for the case of b at ∞) will be referred to as the analytic solution.

Now that the results for an analytic solution of the pressurized tube problem have been presented, various numerical results for this problem will be examined. The first problem to be discussed is that of a pressurized tube modeled solely with finite elements.

Pressurized Tube: Finite Element Model

A numerical solution for a pressurized tube problem has been calculated using a finite element model. The geometry for the problem is the same as that shown for the problem in Figure 1. The value for a for this problem is 10 m, and the value for b is 200 m. With these particular values for the inner and outer radii, the geometry can be used to approximate a cylindrical cavity in an infinite medium. The material for the tube has an elastic modulus, E, of 15,200 MPa, a Poisson's ratio, ν, of 0.35, and plastic hardening modulus of 15.2 MPa. Since the plastic modulus is 0.1% of the elastic modulus, the material in the tube approximates an elastic-perfectly plastic material. The tensile yield stress, σ_y, for the material is 5.0 MPa. The tensile yield stress is related to the shear yield stress in the previous section by

$$\sigma_y = \sqrt{3}\tau_s. \qquad \text{(EQ 17)}$$

Only a quarter of the geometry is used in the finite element model (Figure 2). The proper boundary conditions are applied so that the quarter geometry model simulates a cylindrical tube problem. Edges of the quarter model lie on the radial lines at $\theta = 0$ radians and $\theta = \pi/2$ radians. Along these two radial lines, u_θ is constrained to be zero and u_r is

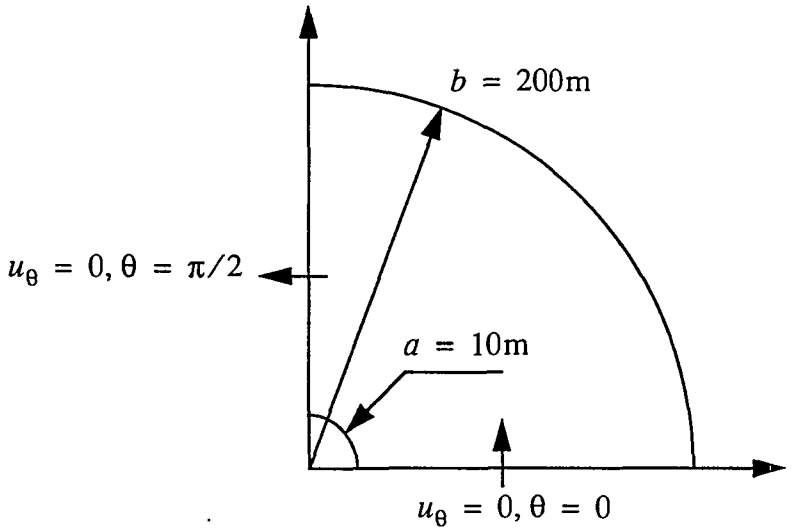

Figure 2. Geometry and Boundary Conditions for Cylindrical Tube Problem Modeled with Finite Elements

unconstrained. The outer surface at $b = 200$ m is unconstrained, and a pressure is applied to the inner surface at $a = 10$ m. The finite element model consists solely of quadrilateral elements. There are 1464 elements in the mesh, and the mesh is graded so that the mesh is finer at the inner radius than at the outer radius. Plane strain conditions specify behavior in the direction of the z axis.

The pressure on the inner surface is increased linearly from 0 to 10 MPa. The finite element problem has been solved with code JAC2D[10]. The radial displacement, u_r, at $r = 10$ and $\theta = 0$ as a function of pressure is presented as a dashed line in Figure 3. Yielding occurs on the inner surface when $p = 5/\sqrt{3}$ MPa, which is approximately 2.8868 MPa. In Figure 3, the radial displacement as a function of pressure begins to vary from a simple linear relation at 2.9 MPa, which is the expected result since nonlinear behavior sets in after yield occurs.

A comparison can be made between the finite element results and the analytic solution presented in previous sections. The calculated value for u_r, at $r = 10$ and $\theta = 0$ as a function of pressure is presented in Figure 3 as a solid line. To obtain this line, Equation (7) for the limiting case of b approaching ∞ is used to calculate u_r at $r = a$ up to the point where yield occurs ($p = 5/\sqrt{3}$ MPa). Once yield occurs, the value for u_r is calculated by using Equations (15) and (16).

Figure 3 shows good agreement between the finite element calculations and the analytic results. Up to a certain point (approximately 6.4 MPa), the radial displacement at the inner surface predicted by the finite element calculations is less than the analytic results. At greater pressures, the radial displacement predicted by the finite element calculations is greater than the analytic results. At 10.0 MPa, the finite element results predict a radial

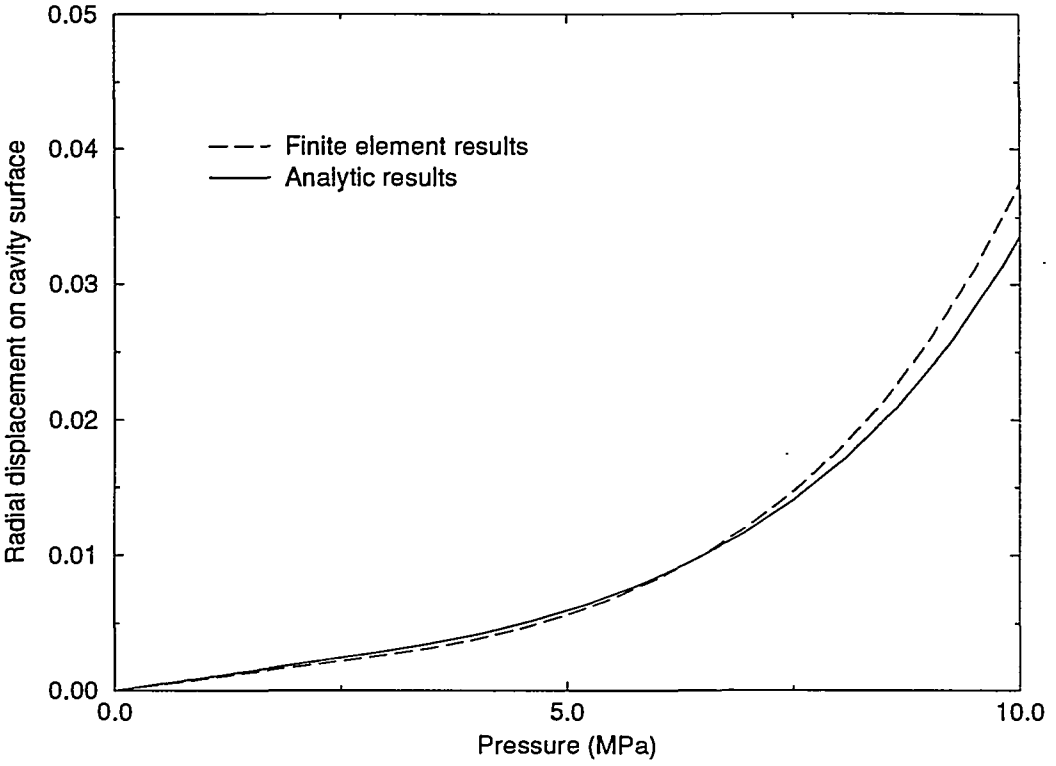

Figure 3. Comparison of Finite Element and Analytic Results (b = 200 m)

displacement of 0.0375 m at the inner surface, and the analytic results predict a radial displacement of 0.0335 m. The two methods vary by approximately 12% at 10.0 MPa. There are several reasons why the finite element and analytic solutions vary. First, the material in the finite element calculations has a Poisson's ratio of 0.35 while the material in the analytic solution is incompressible ($\nu = 0.5$). This difference in Poisson's ratio probably accounts for a significant amount of the differences in the two solutions. Second, the material in the finite element mesh is elastic-plastic; the material in the analytic solution is elastic-perfectly plastic. The parameters in the finite element model are chosen so that the material closely approximates an elastic-perfectly plastic material, which means that the elastic-plastic nature of the material in the finite element model is probably not a significant source of the differences in the two solutions. Finally, the finite element mesh models a finite region while the equations for the analytic solution are for an infinite region. At 10.0 MPa, the elastic-plastic interface is at r = 34.2825 m, which is 17.14% of the outside radius of the finite element model. This is a significant percentage of the outside radius of the finite element mesh. The approximation to an infinite region in the finite element mesh becomes less and less accurate as the elastic-plastic interface moves outward from the inner radius. It accounts for some of the increasing difference in the two solutions past 6.4 MPa.

In order to quantify the effects of the approximation of an infinite region with a mesh with a finite outer radius, a finite element model with an outer radius greater than 200 m was used. The problem shown in Figure 2 was modeled with a value of b = 400 m rather than b = 200 m. The material properties and loading are kept the same and plane strain

conditions are again specified. The number of elements is increased to 2112. The mesh is graded so that it is finer at the inner radius than the outer radius. The radial displacement at the cavity surface from the analysis with $b = 400$ m is shown in Figure 4 as a dotted line.

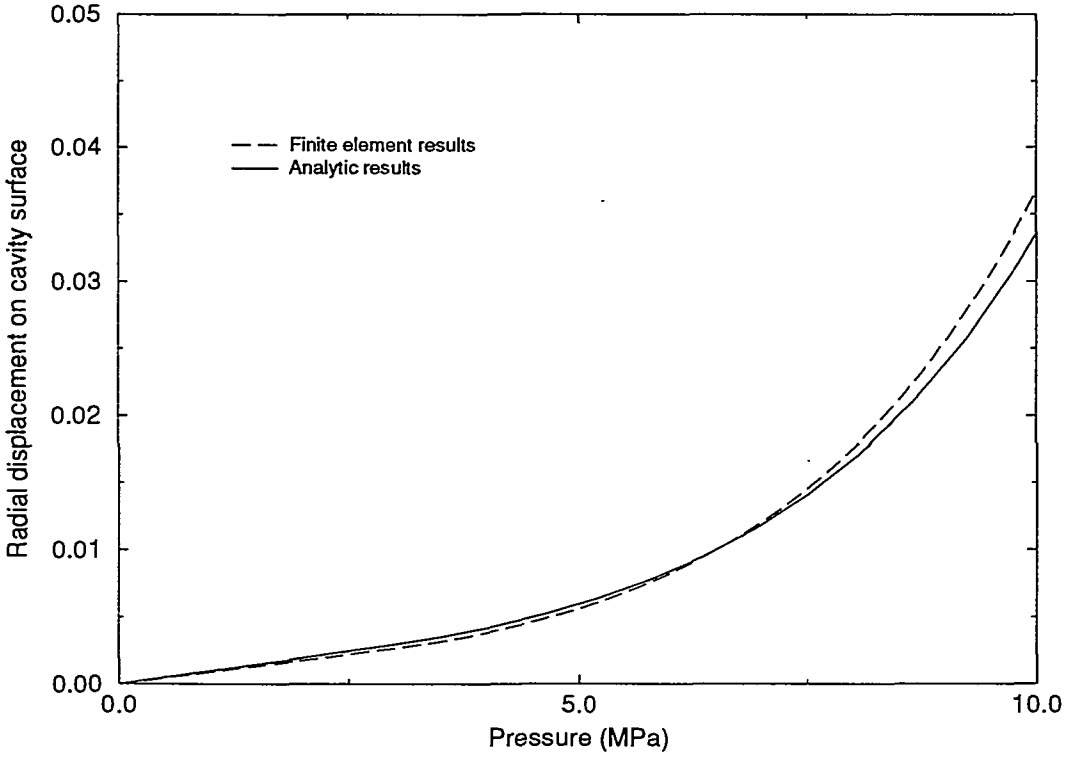

Figure 4. Comparison of Analytic and Finite Element Results ($b = 400$ m)

They are compared with radial displacement results from the analytic solution. The finite element results for the case of $b = 400$ m agree slightly better with the analytic results than the finite element results for the case of $b = 200$ m. At 10.0 MPa, the finite element mesh with $b = 400$ m predicts a radial displacement at the cavity surface of 0.0367 m, which is slightly smaller than the value predicted by the finite element calculations with $b = 200$ m. The percentage difference between the finite element results ($b = 400$ m) and the analytic results is 9.6%. The doubling in value of b leads to only a small adjustment in the difference between the finite element and analytic results. The original mesh does provide a fairly accurate basis of comparison.

On the whole, the finite element and analytic problems produce good agreement. The analytic solution and finite element problem just presented will prove useful for verification of numerical results in the following sections. In subsequent sections, the finite element models with $b = 200$ m and $b = 400$ m consisting only of elastic-plastic material will be referred to as the single material problem since the cavity is surrounded by only one type of material. The following sections discuss the solution of the cylindrical cavity problem where the cavity is surrounded by an elastic-plastic material which is in turn surrounded by an elastic material.

Solution of Nonlinear Cylindrical Cavity Problems Using a Coupled Finite Element/Boundary Element Technique

This section discusses the solution of cylindrical cavity problems with nonlinear behavior by using a coupled finite element/boundary element technique. The cavity is surrounded by a concentric ring of elastic-plastic material, which in turn is surrounded by elastic material. Since the concentric ring of material around the cavity is a nonlinear material, it can easily be modeled with finite elements. The surrounding infinite medium of elastic material is best suited for modeling with boundary elements. This particular problem is well suited for investigation of the use of a coupling technique for problems involving nonlinear material behavior. The coupling technique chosen for solution of the problem is the one described in Reference 9. The finite element method and boundary element method are coupled by enforcing displacement compatibility and force equilibrium at the nodes where the finite element and boundary element regions coincide. The resulting set of equations, which is nonsymmetric, is solved by using a conjugate gradient scheme for nonsymmetric operators (the Bi-CGSTAB method[12]). Conjugate gradient schemes have the advantage that it is not necessary to construct the full stiffness matrix. This eliminates the problem of large storage requirements for large-scale finite element models. They are also an efficient solution scheme for large-scale three-dimensional problems.

All of the problems solved in Reference 9 involve completely elastic material. The problems discussed in this memo examine the coupling scheme when used with problems exhibiting nonlinear material behavior. The results in the following sections will show that the coupling scheme is valid for problems involving nonlinear material behavior. For this class of problems, however, the Bi-CGSTAB method alone is not sufficient as a solution technique for the resulting set of equations. It becomes necessary to use a solution approach based on a Newton scheme[13]. Newton's method is used to set up a linear system of nonsymmetric equations that are solved with the Bi-CGSTAB method. The reasons for using this approach are discussed in the following sections.

Because the problems involve nonlinear material, the load must be applied incrementally. A Newton scheme as outlined in Reference 13 is used to obtain a solution in an incremental manner. For this process, we define the residual R as the difference between the external and internal forces for a system. Let ΔF_{ext} represent the increment in the external load for the current load step, and F_{ext} be the total external load after the load increment ΔF_{ext} is applied. If the value of the internal forces at the beginning of the load step is $F_{int(0)}$, and the tangent stiffness matrix at the beginning of the load step is $K_{T(0)}$, we can estimate a displacement increment Δu_1 corresponding to the current external load increment with the relation

$$\Delta u_1 = K_{T(0)}^{-1}(F_{ext} - F_{int(0)}), \qquad \text{(EQ 18)}$$

where $K_{T(0)}^{-1}$ is the inverse of the tangent stiffness. If u_0 is the displacement at the beginning of the load increment, then the total displacement after Δu_0 is $u_1 = u_0 + \Delta u_0$. The set of internal forces, $F_{int(1)}$, corresponding to the displacements u_1 is, in general, not equal to F_{ext} for nonlinear problems. The calculation in Equation (18) is repeated in the general form

$$\Delta u_{i+1} = K_{T(i)}^{-1}(F_{ext} - F_{int(i)}) \qquad \text{(EQ 19)}$$

until some measure of the difference $F_{ext} - F_{int(i)}$ is smaller than a prescribed tolerance. If this difference is small enough after n iterations, then the displacement, u_n, corresponding to F_{ext} is given by

$$u_n = u_0 + \sum_{i=1}^{n} \Delta u_i. \qquad \text{(EQ 20)}$$

The Newton scheme establishes a set of equations of the form

$$K_{T(i)}\Delta u_{i+1} = F_{ext} - F_{int(i)}. \qquad \text{(EQ 21)}$$

for each iteration within a load step. In the coupled scheme, the system of equations given by Equation (21) is solved using the Bi-CGSTAB method. The tangent stiffness matrix in Equation (21) is nonsymmetric, and the Bi-CGSTAB method is capable of solving such a system of equations through an iterative process. In order to obtain a solution for a displacement increment, Δu_i, with the Bi-CGSTAB method, a series of orthogonal basis vectors is constructed[12]. Implicit in this iterative process is a constant tangent stiffness. During the iterative process within the Bi-CGSTAB method, the value for $K_{T(i)}$ remains constant.

The Bi-CGSTAB solver differs from the conjugate gradient technique in JAC2D in that the tangent stiffness for the conjugate gradient technique in JAC2D can vary during the computation of a displacement increment[14,15]. The version of the conjugate gradient method in JAC2D is limited, however, to problems where the tangent stiffness matrix is very nearly symmetric, which makes it impractical for the coupled scheme. In JAC2D, the value for $K_{T(0)}$ in the system of equations

$$K_{T(0)}\Delta u_1 = F_{ext} - F_{int(0)} \qquad \text{(EQ 22)}$$

varies with each iteration for the conjugate gradient technique. It is possible to obtain the solution for a displacement increment corresponding to an entire load increment ΔF_{ext} by

a single application of the conjugate gradient solution technique in JAC2D. For the coupled scheme, it is necessary to break the load increment into a set of linear equations as described by Equation (21). Each set of equations is solved by the Bi-CGSTAB method.

Several attempts were made to solve problems involving nonlinear material behavior by solving the resulting system of equations using only the Bi-CGSTAB method for each load increment. The Bi-CGSTAB method would not converge to a solution for load steps at the onset of nonlinear material behavior. When the Newton solver was used to break the load increment into a sequence of linear equations, however, it was possible to obtain solutions for load steps after the onset of nonlinear material behavior.

Three cylindrical cavity problems involving nonlinear material behavior have been solved by using the coupled scheme with a Newton solver. The only difference among the problems is the radius at which the interface between the elastic-plastic material and elastic material occurs. The choice for the boundary of the interface between the elastic and elastic materials is arbitrary. Three different values for the interface radius were used to provide a reasonable check of the numerical techniques used for solving the problems.

For the first problem, the inner radius for the cavity, a, is at 10.0 m and, the radius defining the interface between the elastic-plastic and elastic materials, r_i, is at 16 m. The geometry for this particular problem is shown in Figure 5. The properties for the elastic-plastic

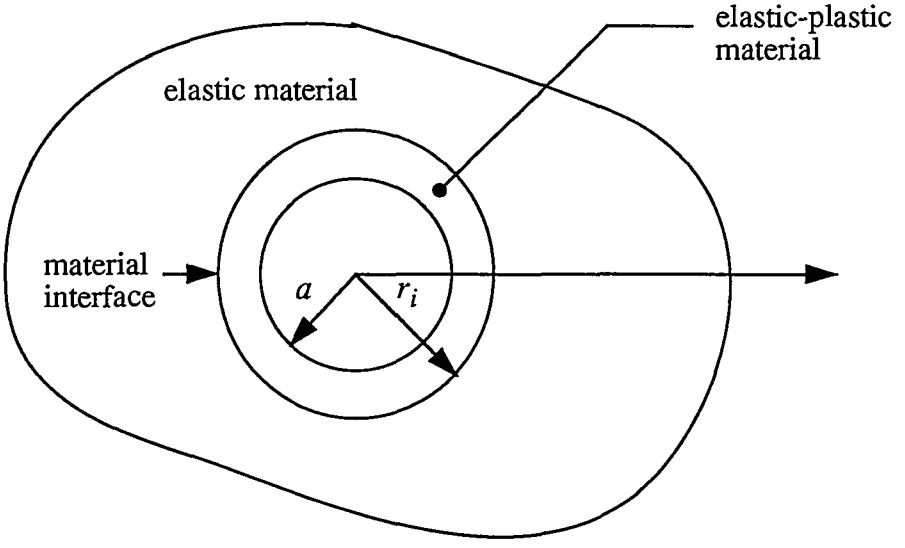

Figure 5. Geometry for Cylindrical Cavity Problem for Two Materials

material are the same as the ones used for the single material problem in the preceding section. The elastic-plastic material surrounding the cavity has an elastic modulus of 15,200 MPa and a Poisson's ration of 0.35. The plastic modulus for this inner material is 15.2 MPa, and the tensile yield stress is 5.0 MPa. The elastic material surrounding the elastic-plastic material has an elastic modulus of 15,200 MPa and a Poisson's ratio of 0.35. The pressure inside the cavity is increased linearly from 0.0 MPa to 10.0 MPa.

The mesh for the solution of this problem with the coupled scheme is shown in Figure 6.

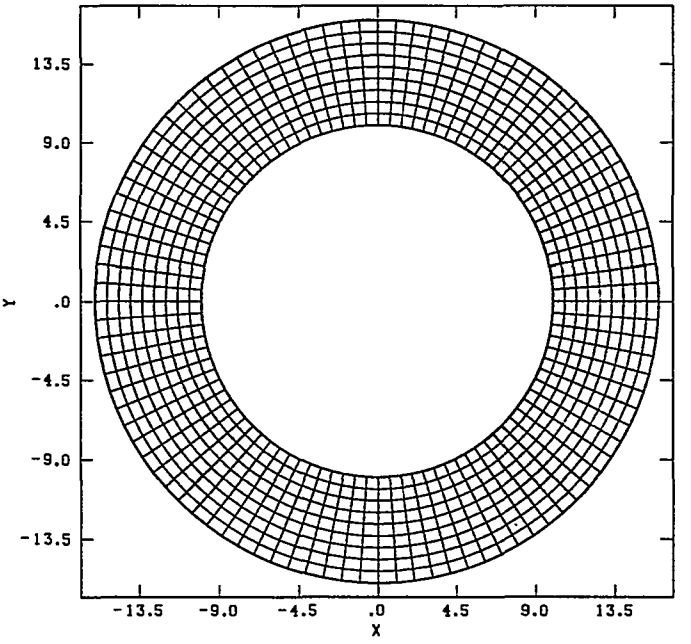

Figure 6. Mesh for Coupled Problem with Material Interface at $r = 16$ m

The interior elastic-plastic material is modeled with finite elements. The elastic material is modeled by a boundary element contour that corresponds to the outer surface of the finite element mesh at $r = 16$ m. A boundary element coincides with each element edge defining the outer surface of the finite element mesh. The boundary element nodes correspond to the finite element nodes. No use is made of symmetry in the problem. The current version of the coupled scheme is still experimental code, and it has not been enhanced to exploit symmetry in problems. (The coupling scheme does allow for the implementation of schemes that exploit symmetry in problems.)

The radial displacement, u_r, at the cavity wall ($r = 10$, $\theta = 0$) is plotted as a function of pressure in Figure 7 for the coupled problem. These results from the coupled problem can be verified by use of a finite element model with elastic-plastic material response in the region $10\text{m} < r < 16\text{m}$ and elastic response in the region $16\text{m} < r < 200\text{m}$. The large outer radius approximates the infinite extent of the region. The finite element results are also plotted in Figure 7 as a dashed line. As can be seen in Figure 7, the coupled finite element/ boundary element results agree quite well with the finite element results.

The coupled results in Figure 7 are not carried out fully to 10.0 MPa. It was difficult to achieve convergence for the coupled problem past 8.4 MPa. This particular problem is actually somewhat difficult to solve by use of conjugate gradient techniques. The elastic-plastic material becomes quite soft after yield, and conjugate gradient techniques can have difficulty converging to solutions for problems with soft materials. A solution was obtained for the model involving only finite elements up to pressure 10.0 MPa. This

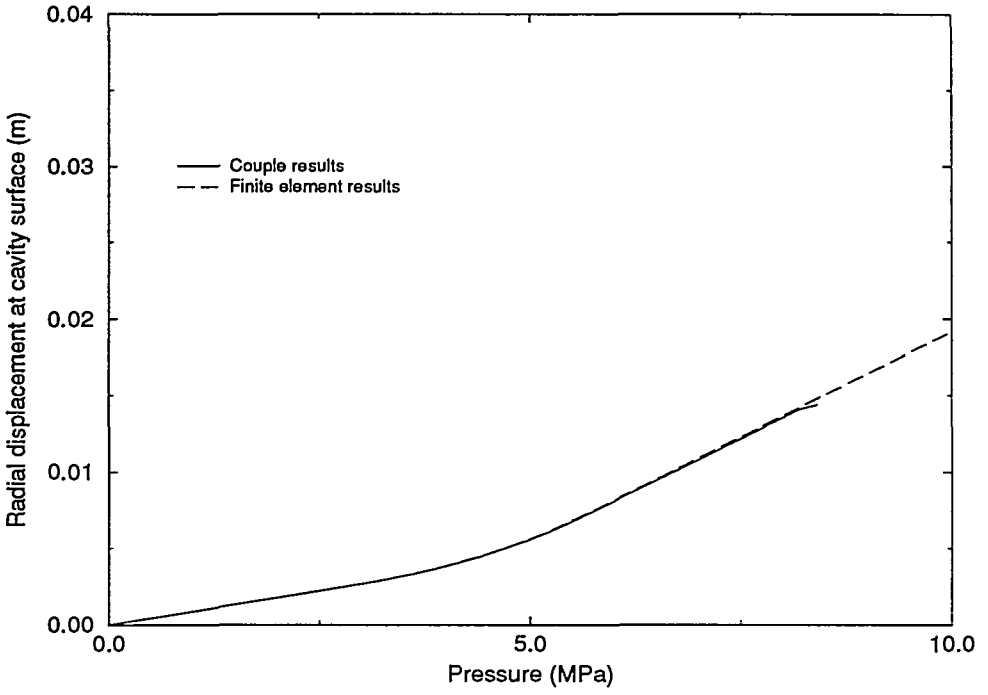

Figure 7. Comparison of Coupled and Finite Element Model Results for Cylindrical Cavity Problem with Material Interface at 16 m

problem was solved using the standard conjugate gradient technique in JAC2D. There is more experience with the use of the standard solution method in JAC2D than the solution method for the coupled scheme. Rather than refine the load increments for the coupled problem so that it ran to 10.0 MPa, the problem was run only to a point where significant nonlinear behavior occurred so as to establish accuracy for the coupled scheme.

It should be noted that the final solution for the coupled problem obtained by use of the Bi-CGSTAB method was substantially past the point where the plastic zone reached the material interface. At 8.2 MPa, the coupled problem produced a radial displacement of 0.01409 m at the cavity surface, and the finite element model produced a radial displacement of 0.01423 m at the cavity surface. The coupled solution and finite element solution differ by only 0.93%.

The coupled results can also be verified by comparison with the problem of a cylindrical cavity surrounded by an elastic-plastic material only. The coupled results should agree with the results for the problem with elastic-plastic material only up to the point where the interface between the plastic zone and elastic zone is less than the material interface in the coupled problem. After this, the results for the coupled problem and the single material problem should begin to diverge. It is possible to use the analytic solution for the pressurized cylindrical cavity to estimate the pressure at which the interface between the plastic zone and elastic zone, c, will reach the material interface at r_i. Equation (14) gives the pressure in the cavity for a given value of c. When $c = r_i$, the interface between the

plastic zone and elastic zone reaches the material interface. The pressure at which the interface between the plastic zone and elastic zone reaches the material interface ($c = r_i$) is $p = 5.6$ MPa.

Figure 8 shows the radial displacement, u_r, at the cavity wall ($r = 10$, $\theta = 0$) for the coupled problem. Also shown in Figure 8 are the results from the finite element model (b

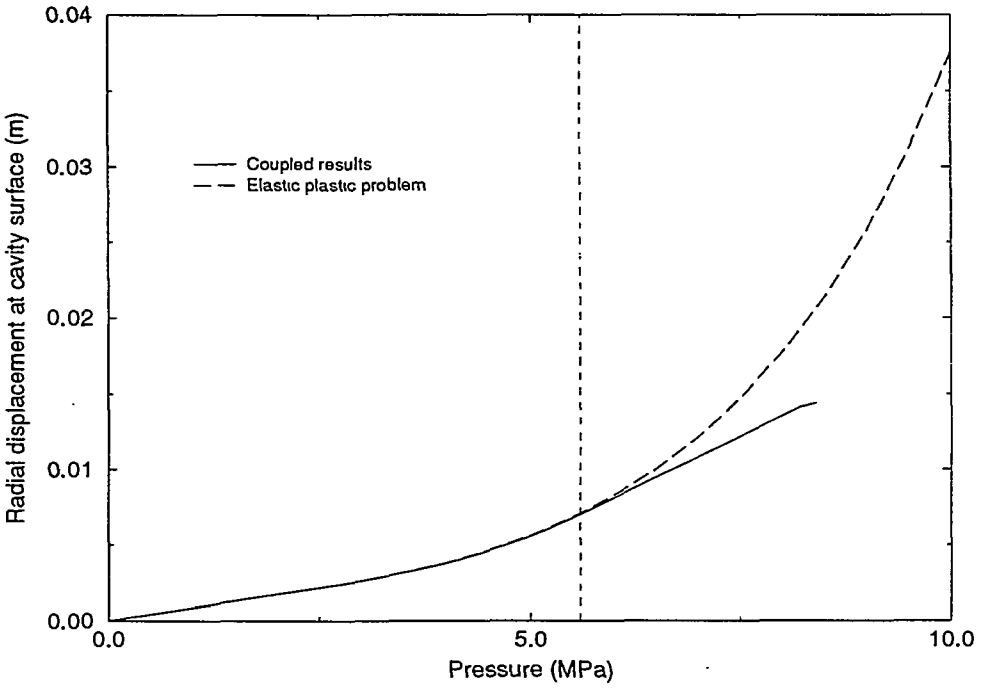

Figure 8. Comparison of Coupled Results with Material Interface at 16 m with Results from Cavity in Elastic-Plastic Medium Only

= 200 m) for the single material problem. These are the same finite element results that are shown in Figure 3. The two material (coupled) problem results shown in Figure 8 begin to diverge from the single material results at 5.6 MPa, the pressure predicted by the analytic problem. (A vertical dashed line has been drawn in Figure 8 to mark 5.6 MPa.) Although the analytic problem varies slightly from the problem defined for the numerical study, it predicts the point of divergence fairly close in Figure 8.

It is important to note that both of the verification procedures just discussed involve some approximate comparisons. The analytic problem is slightly different from the two numerical models. The finite element model with the large outer radius only approximates an infinite region. The differences among the problems used for comparison are slight, however, and do not contribute to substantial differences in behavior. The problems are similar enough so that one can conclude that the coupled scheme is producing accurate results.

For the second problem to study the coupled scheme with problems involving nonlinear material behavior, the preceding problem is modified so that the interface between the elastic-plastic material and elastic material is at $r = 27$ m. This is the only change made for this second problem. All other geometry and material parameters used for the first coupled problem remain the same.

The mesh used to model this second problem for the coupled scheme is shown in Figure 9.

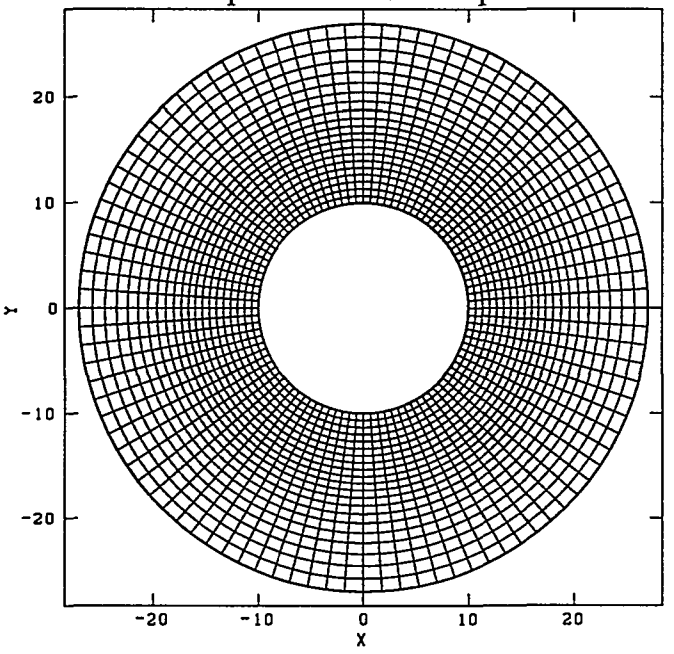

Figure 9. Mesh for Coupled Problem with Material Interface at r = 27 m

The interior elastic-plastic material is modeled with finite elements. The elastic material is modeled by a boundary element contour that corresponds to the outer surface of the finite element mesh at $r = 27$ m. A boundary element coincides with each element edge defining the outermost surface of the finite element mesh. The boundary element nodes correspond to the finite element nodes. As in the previous case, no use is made of symmetry.

The radial displacement, u_r, at the cavity wall ($r = 10$, $\theta = 0$) is plotted as a function of pressure in Figure 10 for the coupled problem. The results from this coupled problem can also be verified by use of a finite element model with a large outer radius to approximate an infinite medium. The same finite element model of a thick-walled tube used for verification of the previous problem is also used for verification of this coupled problem. The finite element mesh used to verify the current problem has a material interface embedded in the finite element mesh between the elastic-plastic and elastic material at $r =$ 27 m. The finite results are plotted in Figure 10 as a dashed line. As can be seen in Figure 10, the coupled results agree quite well with the finite element results. At 10.0 MPa, the coupled problem predicts a radial displacement at the cavity surface of 0.03333 m and the

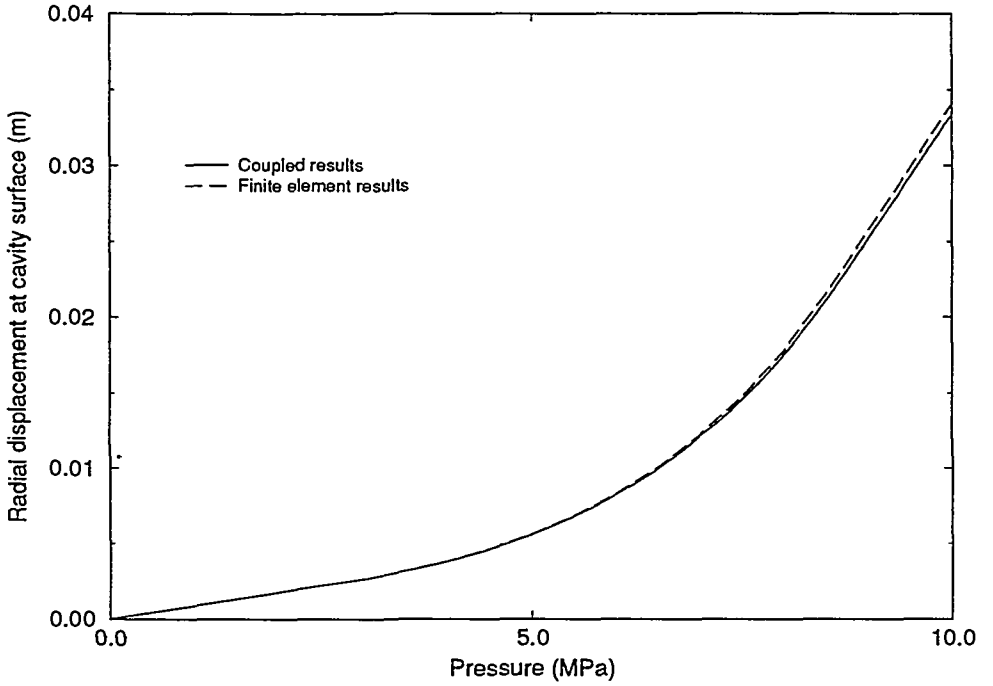

Figure 10. Comparison of Coupled and Finite Element Model Results for Cylindrical Cavity Problem with Material Interface at 27 m

finite element model predicts a radial displacement at the cavity surface of 0.03405 m. The predictions for the radial displacement agree to within 2.16%.

This second coupled problem can also be verified by comparison with the problem of a cylindrical cavity surrounded by an elastic-plastic material only. As before, the analytic solution for a pressurized tube is used to calculate the pressure at which the radius of the plastic zone will coincide with the material interface. By using Equation (14), it can be determined that the radius of the plastic zone is approximately equal to the material interface radius of $r = 27$ m when the pressure in the cavity is 8.6 MPa. At this pressure, the results from the coupled problem with a material interface at $r = 27$ m should begin to diverge from the results from the problem where the cavity is surrounded by elastic-plastic material only. A plot of results for the coupled problem and the single material problem ($b = 200$ m) is shown in Figure 11. The results from the two problems do diverge at the correct pressure. A vertical dashed line in Figure 11 marks the 8.6 MPa point.

As a final check, a problem with the material interface at $r = 40$ m has been run using the coupled scheme. As in the previous cases, the annulus surrounding the cavity and up to a radius of 40 m is elastic-plastic, and the surrounding medium is elastic. The properties of the two materials are the same as in the previous two problems. The cavity is again pressurized to a maximum value of 10 MPa. According to the analytic solution, when the cavity pressure reaches 10 MPa, the interface between the plastic zone and elastic zone will be at 34.28 m. Since the material interface in the model is greater than 34.28 m, the interface between the plastic and elastic zones will not reach the material interface for this

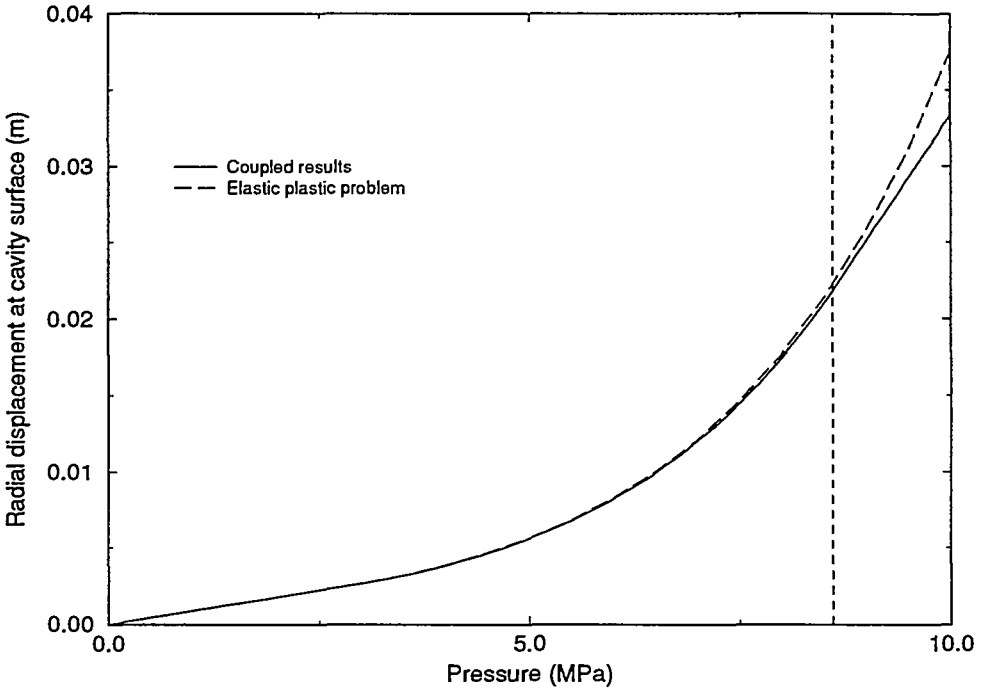

Figure 11. Comparison of Coupled Results with Material Interface at 27 m with Results from Cavity in Elastic-Plastic Medium Only

particular problem. As a result, the coupled model with a boundary element contour at r = 40 m should agree with the single material problem up to 10.0 MPa.

Figure 12 shows results for this particular problem. The model for the coupled problem is similar to the ones shown in Figures 6 and 9. A finite element mesh is used to model the annulus of elastic-plastic material. There is a boundary element contour at r = 40 m. The radial displacement u_r at the cavity surface as predicted by the coupled scheme is plotted as a solid line in Figure 12. The radial displacement at the cavity surface for the single material model (b = 400 m) is plotted as a dashed line in Figure 12. As can be seen from the graphical output, the coupled solution and single material solution (finite elements only) agree quite well. The coupled approach predicts a radial displacement of the cavity surface of 0.03639 m at 10.0 MPa, and the single material solution (b = 400 m) predicts a radial displacement of the cavity surface of 0.03667 m. The two solution methods agree to within 0.76%.

For this last verification problem, the single material model used a value of b = 400 m rather than the b = 200 m used in the previous check problem with a material interface at 27 m. Since this last verification problem has a larger value for the material interface (40 m) than the previous problem, it was assumed that the larger value for b would be necessary for more reliable results.

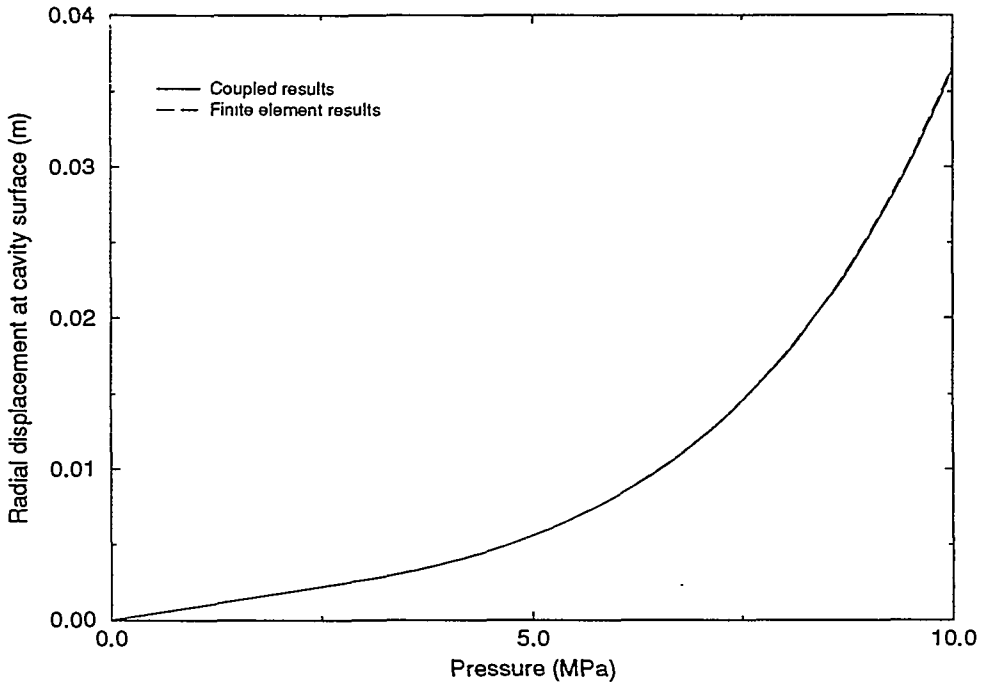

Figure 12. Comparison of Coupled and Finite Element Model Results for Cylindrical Cavity Problem with Material Interface at 40 m

Jointed Rock Problems

The second nonlinear material model used for coupled problems is a jointed rock model[16-18]. Results are presented from problems with two different geometric configurations in order to assess the accuracy of the coupled scheme. Both of these problems model a pressurized circular cavity surrounded by an annulus of jointed rock material. The annulus is surrounded by an infinite medium of elastic material. The radius at which the interface between the two materials occurs is different for the two problems.

Pressurized Circular Cavity: Material Interface at 16 m

The general geometry for two problems is shown in Figure 13. The radius for the cavity is denoted by a, and the radius for the material interface is denoted by r_i. For the first problem, r_i is set to 16 m.

The jointed rock material surrounding the cavity has orthogonal joint sets. The joints in a given set are assumed to be regularly spaced and parallel. The orientation for the joint sets for both problems is shown in Figure 13. One set of joint planes is parallel to the x axis, and the other set of joint planes is parallel to the y axis. The joint planes are characterized

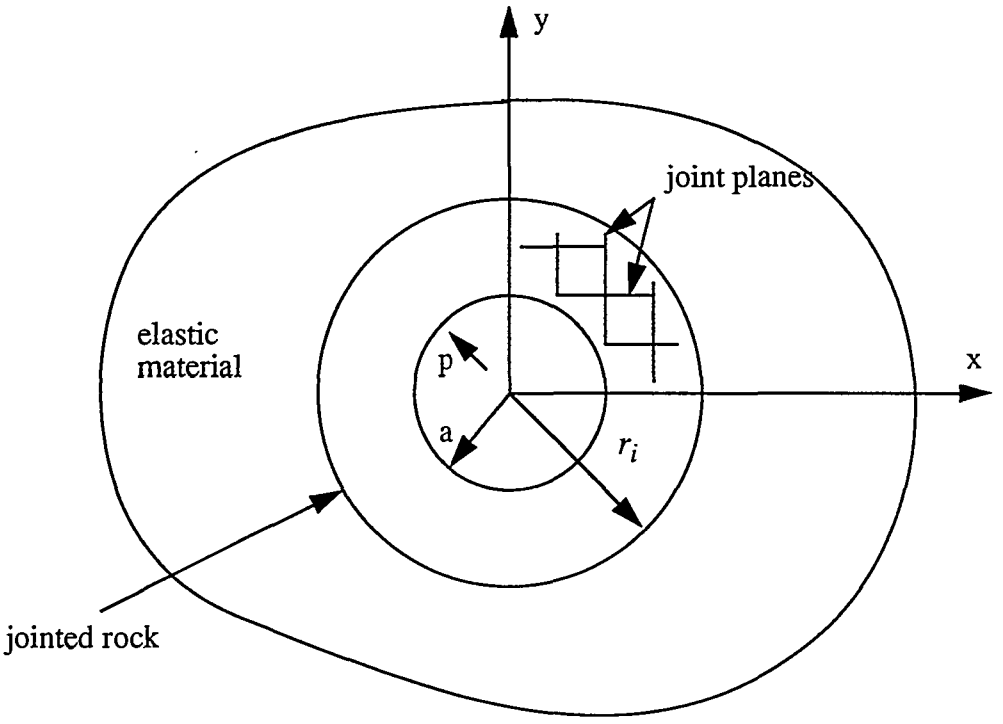

Figure 13. Geometry for Cylindrical Cavity Problem

by their unit normal vectors. The joint set parallel to the y axis is associated with the normal vector $\underset{\sim}{m}$, which is parallel to the x axis. The joint set parallel to the x axis is associated with the normal vector $\underset{\sim}{n}$, which is parallel to the y axis. Properties of the joint set with the normal $\underset{\sim}{m}$ have a subscript of m, and properties of the joint set with normal $\underset{\sim}{n}$ have a subscript of n.

A number of parameters are required to describe the properties for the jointed rock material. (A full description of these parameters is given in Reference 16.) The material between the joint planes is assumed to be linear elastic, and is characterized by an elastic modulus, E, and a Poisson's ratio, ν. The spacing for the joint set with normal $\underset{\sim}{m}$ is δ_m, and the spacing for the joint set with normal $\underset{\sim}{n}$ is δ_n. Displacements normal to a joint plane k, where k can be m or n, in the direction normal to a joint plane is governed by the relation

$$u_k = \frac{U_{max,\,k}\sigma_{normal,\,k}}{(\sigma - A_k)}, \qquad \text{(EQ 23)}$$

where $\sigma_{normal,\,k}$ is the stress normal to the joint plane and u_k is the measure of the joint opening (or closure). As the joint opens, the maximum stress across the joint plane asymptotically approaches an upper limit, A_k. As the joint closes, the joint closure

asymptotically approaches a maximum closure value, $U_{max,k}$. For joint set m, the maximum tensile stress that can be carried by the joints is denoted by A_m, and the maximum joint closure is denoted by $U_{max,m}$. The analogous quantities for joint set n are A_n and $U_{max,n}$. Slip across a joint plane k is governed by a slip displacement, $u_{slip,k}$, versus shear stress behavior, $\sigma_{shear,k}$, that is bilinear with a transition from elastic to inelastic behavior governed by a Mohr-Coulomb failure criterion. The relation between the slip and shear stress across a joint plane k is

$$u_{slip,k} = \frac{\sigma_{shear,k}}{G_k} \qquad \text{(EQ 24)}$$

for elastic behavior and

$$u_{slip,k} = \frac{\sigma_{shear,k}}{G_k'} \qquad \text{(EQ 25)}$$

for inelastic behavior. The joint shear stiffness is G_k in the elastic range and G_k' in the inelastic range. A scalar slip function is defined by

$$F_k = |\sigma_{shear,k}| + \mu_k \sigma_{shear,k} - C_{0,k}. \qquad \text{(EQ 26)}$$

In Equation (26), μ_k is the coefficient of friction for the joint plane, and $C_{0,k}$ is the joint plane cohesion. The joint slip behavior is elastic if $F \leq 0$ and inelastic if $F > 0$. For joint set m, the elastic shear stiffness is G_m, the inelastic shear stiffness is G_m', the coefficient of friction is μ_m, and the joint cohesion is $C_{0,m}$. The analogous quantities for joint set n are G_n, G_n', μ_n, and $C_{0,n}$.

The effects of a joint plane in a set are averaged over the distance separating the planes in that set. With this approach, the effects of the joint planes can be incorporated into a continuum model, which is the technique used for the jointed rock model in these studies.

For the first problem, the elastic modulus of the matrix material, E, is 30.4×10^3 MPa and Poisson's ratio, ν, is 0.24. For joint set m, the maximum closure, $U_{max,m}$, is -3×10^{-5} m, the maximum joint tensile stress, A_m, is 2.0 MPa, the elastic joint shear stiffness, G_m, is 1×10^6 MPa/m, the inelastic joint shear stiffness, G_m', is 10.0 MPa/m, the friction coefficient, μ_m, is 0.54, and the joint cohesion, $C_{0,m}$, is 0.1 MPa. The analogous properties for joint set n have the same values. The spacing for joint set m, δ_m, is 1.0 m,

and the spacing for joint set n, δ_n, is 0.1 m. The elastic material surrounding the jointed rock material has an elastic modulus of 15.2×10^3 MPa and a Poisson's ratio of 0.24. These values are based on values used in some studies done for the Yucca Mountain Project[19,20].

The cavity is pressurized to a value of 1.0 MPa, and there are no initial stresses in the jointed rock annulus or in the elastic material. The final internal pressure of 1.0 MPa represents a significant pressurization of the cavity. Both the finite element and coupled solutions required substantial computer time because of the highly nonlinear behavior of the jointed rock model. The computer time required to obtain solutions for a 1.0 MPa pressure is large. No attempts were made to obtain solutions greater than 1.0 MPa.

The problem has been modeled by using a finite element model only. The finite element mesh has an outer radius, b, of 200 m. This value is large in comparison to the cavity radius and the material interface radius so that the model reasonably approximates the case of a infinite elastic medium surrounding the jointed rock model annulus. Only a quarter of the geometry is used for the finite element model (Figure 14). Edges of the model lie along the

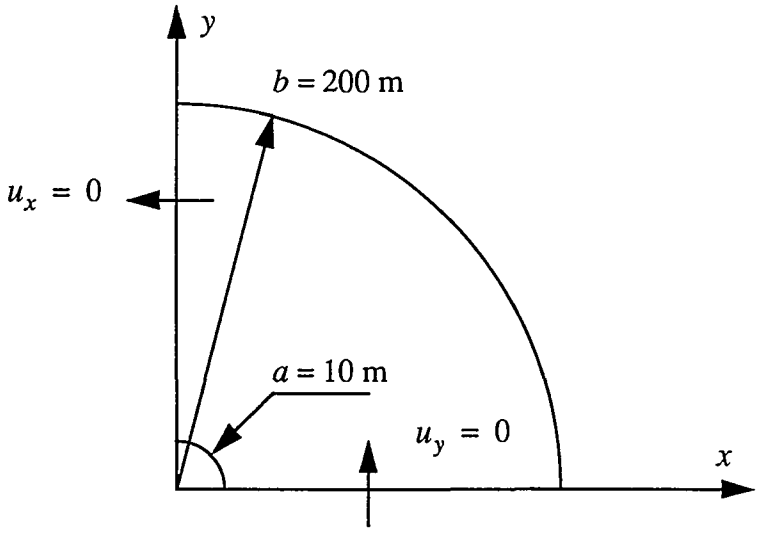

Figure 14. Geometry and Boundary Conditions for Finite Element Model for Circular Cavity Problems (Not to Scale)

positive x and y axes. The edge of the model along the x axis is constrained so that $u_y = 0$, and the edge of the model along the y axis is constrained so that $u_x = 0$. The outer surface at $b = 200$ m is unconstrained, and the surface of the cavity is subjected to pressure, p. The finite element model consists solely of quadrilateral elements. There are 1464 elements in the mesh, and the mesh is graded so that the mesh is finer at the inner radius than at the outer radius. Plane strain conditions specify the behavior normal to the xy plane.

The problem has also been modeled by using a combined finite element and boundary element mesh. The mesh for this model is shown in Figure 15. The interior annulus of

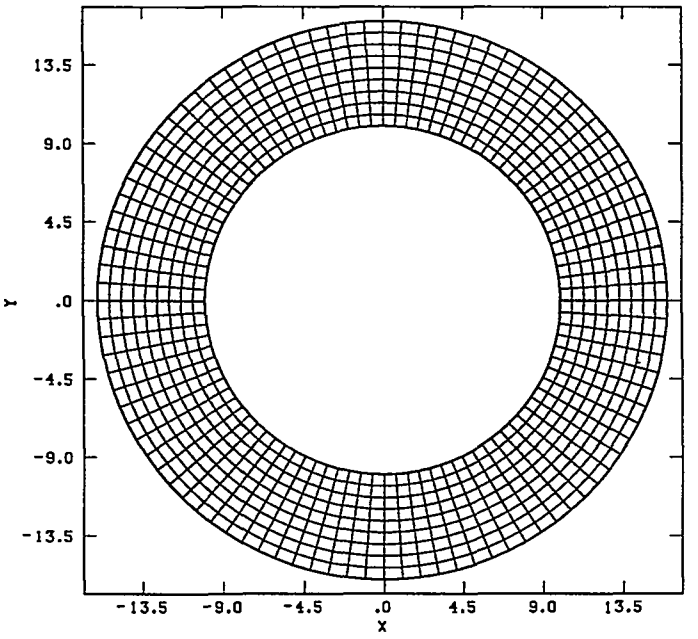

Figure 15. Mesh for Coupled Problem with Material Interface at 16 m

jointed rock material is modeled with finite elements. The elastic material is modeled by a boundary element contour that corresponds to the outer surface of the finite element mesh at r_i = 16 m. A boundary element coincides with each element edge defining the outer surface of the finite element mesh. The boundary element nodes correspond to the finite element nodes. No use is made of symmetry in the problem, because the code being used for solution of the coupled problems is still experimental and has not been enhanced to exploit symmetry in problems.

Results for the model consisting only of finite elements are compared to the coupled results as a means of checking the validity of the coupled results. There is no exact analytic solution for this problem (or even an analytic solution that approximates the problem well) because of the complexity of the jointed rock model and the biaxial nature of the problem. Comparisons of the coupled results with finite element results are the primary means of validation of the coupled results. The finite element results are obtained with the code JAC2D.

Figure 16 compares the displacement in the x direction, u_x, for the point on the cavity surface lying on the x axis as a function of pressure at the cavity surface for the finite element and coupled models. The graphs for the finite element and coupled results follow each other closely, and they cross over each other at several points. From approximately

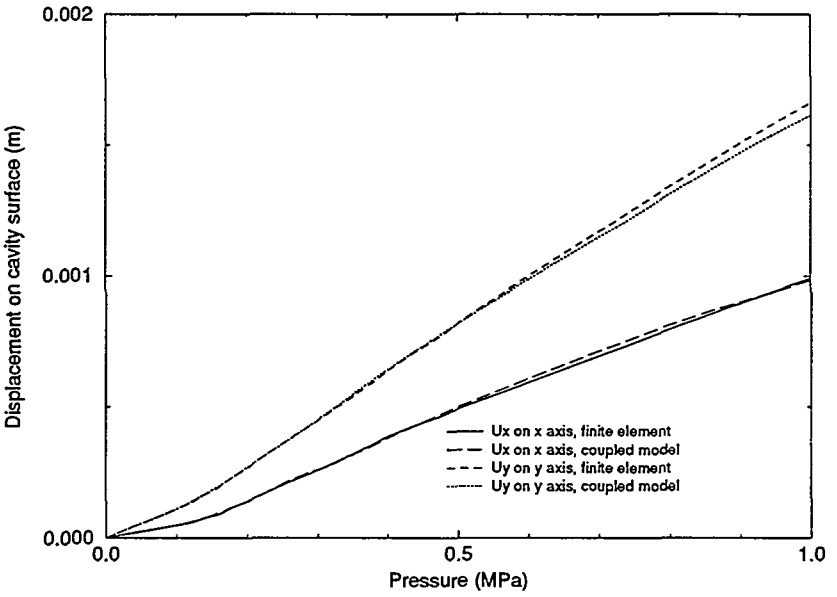

Figure 16. Comparison of Coupled and Finite Element Displacement Results at Points on the Cavity Surface (Material Interface at 16 m)

0.3 MPa to 0.5 MPa, the displacements for the coupled results are less than the displacements for the finite element results. From approximately 0.5 MPa to 0.9 MPa, the displacements for the coupled results are greater than the displacements for the finite element results. The point at approximately 0.9 MPa marks another crossover point. This behavior is probably due to the different solution schemes used to obtain the finite element results and coupled results. As indicated earlier, JAC2D uses a conjugate gradient technique where the tangent stiffness varies over each iteration within a load increment. For each iteration within a load increment, the conjugate gradient routine calls the material routines and generates a new tangent stiffness matrix. The solver used for the coupled problems operates in a different manner. The coupled approach uses a Newton scheme to calculate a series of displacement increments corresponding to a load step. For each iteration in the Newton scheme, a system of linear equations is set up that is solved by the Bi-CGSTAB method. With the Newton scheme in the coupled approach, the tangent stiffness is constant for each Newton iteration within a load step. The Bi-CGSTAB method does not call material routines each time it iterates. It uses the tangent stiffness matrix calculated at the beginning of the Newton increment throughout the iterative process. The results from the jointed rock model are highly path dependent since both the joint normal behavior and slip behavior are nonlinear. The differences in the results for the finite element and coupled methods undoubtedly reflect some path dependent effects introduced by differences in the solution techniques. The differences are quite small however. At 1.0 MPa, the coupled model predicts a value of 9.8298×10^{-4} m for u_x at the point on the cavity

surface on the x axis. The finite element model predicts a value of 9.9141×10^{-4} m, which is a difference of 0.8%.

Figure 16 also shows a comparison of the displacement in the y direction, u_y, for the point on the cavity surface lying on the y axis as a function of pressure at the cavity surface for the finite element and coupled models. The finite element and coupled results show good agreement. The graphs for u_y have several cross-over points, which is similar behavior displayed by the graphs for u_x shown in Figure 16. The variations between the coupled and finite element results for u_y are also due undoubtedly to the path dependent effects introduced by differences in the solution techniques. At 1.0 MPa, the coupled model predicts a value of 1.6161×10^{-3} m for u_y at the point on the cavity surface on the y axis. The finite element model predicts a value of 1.6650×10^{-3} m, which is a difference of 2.9%.

The curves for u_x and u_y in Figure 16 are dissimilar, which is to be expected. The joint spacing for the two joint sets is different, and this introduces directional effects. The geometry is symmetric about both the x and y axes, but the material properties are not.

Figure 17 shows a comparison of the normal stress in the x direction, σ_{xx}, for the element at the cavity surface and adjacent to the x axis for the coupled and finite element models. The values for the normal stress are calculated at the centroid of the element, which means that the location for the stress shown in Figure 17 is close to the surface of the cavity, but not on the surface of the cavity. Because of the location of the stress shown in Figure 17, one would expect it to roughly approximate the applied pressure at the cavity surface. These graphs in Figure 17 show these expected results. The stress in the graphs at any point is close to the value of the applied pressure. The nonlinear behavior of the jointed rock model introduces a slight perturbation in the stress results in the applied pressure range of approximately 0.3 to 0.4 MPa. This perturbation is probably due to the influence of slip displacements on the joint planes. The slip displacements transition from an elastic to inelastic response. As to how this occurs in this problem is a complex process since there is a symmetric geometry and preferential material directions. The transition in slip behavior is probably reflected in the normal stresses as the perturbation seen in Figure 17. Both the coupled and finite element results show this perturbation. The coupled and finite element results show close agreement over the entire applied pressure range from 0 to 1.0 MPa. At a pressure of 1.0 MPa, the value for σ_{xx} for the cavity surface element adjacent to the x axis is -0.9399 MPa for the coupled model. The value for finite element model is -0.9339 MPa, which is a difference of 0.6%.

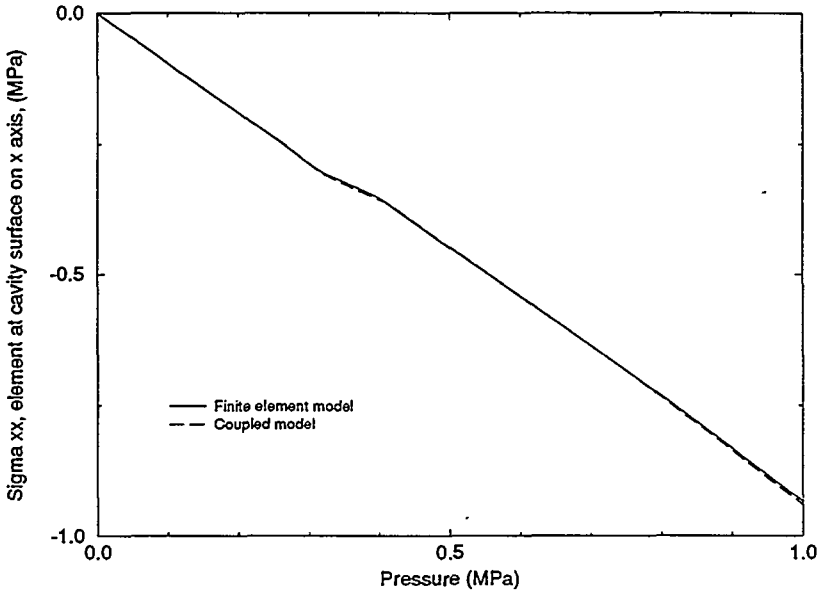

Figure 17. Comparison of Coupled and Finite Element Stress Results for an Element on the Cavity Surface (Material Interface at 16 m)

Pressurized Circular Cavity: Material Interface at 27 m

For the second problem used to study the coupled method for problems involving jointed rock material, the first problem is modified so that the interface between the jointed rock and elastic material is at $r_i = 27$ m. This is the only change made. All other geometry and material parameters used for the first problem remain the same. The cavity is pressurized to a maximum value of 0.5 MPa. The previous problem indicated that most of the significant nonlinear behavior near the cavity wall occurred below 0.5 MPa. Past 0.5 MPa, the displacements near the cavity wall showed almost a linear increase with the increase in pressure. For this larger problem, it was decided to take the solution only up to a point that included the most significant nonlinear behavior plus the transition to the uniform (linear) behavior at 0.5 MPa.

The mesh used to model this second problem for the coupled scheme is shown in Figure 18. The interior jointed rock material is modeled with finite elements. The elastic material is modeled by a boundary element contour that corresponds to the outer surface of the finite element mesh at $r_i = 27$ m. A boundary element coincides with each element edge defining the outermost surface of the finite element mesh. The boundary element nodes correspond to the finite element nodes. As in the previous coupled model, no use is made of symmetry.

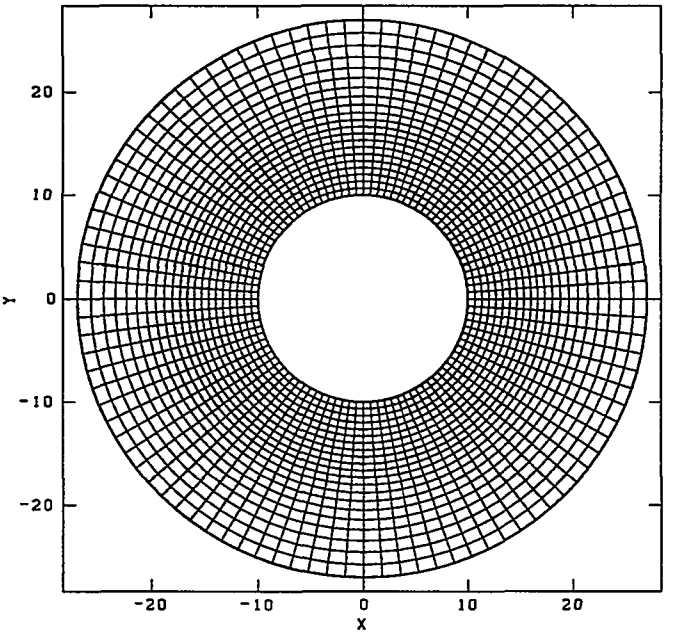

Figure 18. Mesh for Coupled Problem with Material Interface at 27 m

Results from a finite element model are also used to check the validity of the results from the second coupled problem. The finite element model uses the geometry and boundary conditions shown in Figure 14. There is an interface between the jointed rock material and elastic material in the finite element model at $r_i = 27$ m.

Figure 19 compares the displacement in the x direction, u_x, for the point on the cavity surface lying on the x axis as a function of pressure at the cavity surface for the finite element and coupled models. The graphs for the finite element model and coupled results follow each other closely. They cross over each other several times, which is similar to the behavior exhibited in the previous problem. At 0.5 MPa, the coupled model predicts a value of 4.7037×10^{-4} m for u_x at the point on the x axis on the cavity surface. The finite element model predicts a value of 4.9130×10^{-4} m, which is a difference of 4.2%. Figure 19 also compares the displacement in the y direction, u_y, for the point on the cavity lying on the y axis as a function of pressure at the cavity surface for the finite element and coupled models. The graphs of u_y for the two different models are very close. At 0.5 MPa, the coupled model predicts a value of 1.2485×10^{-3} m for u_y at the point on the y axis on the

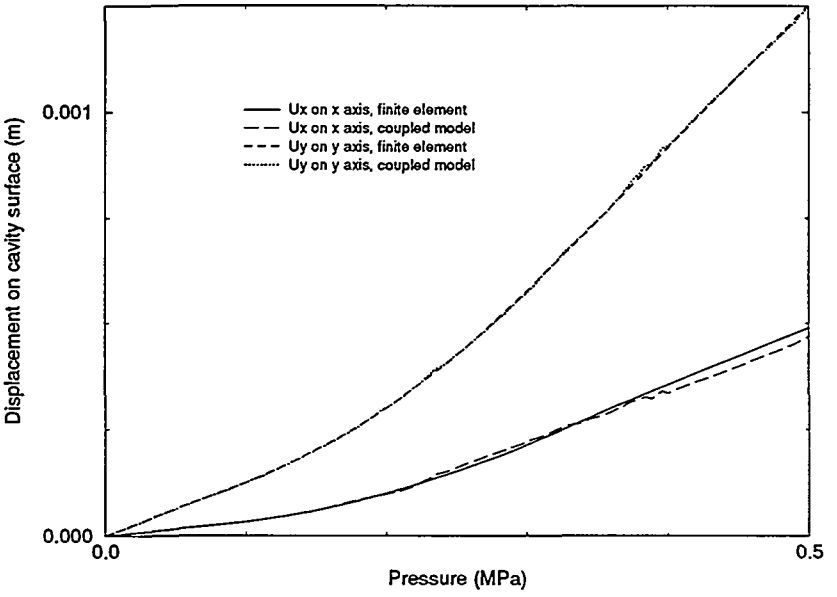

Figure 19. Comparison of Coupled and Finite Element Displacements at Points on the Cavity Surface (Material Interface at 27m)

cavity surface. The finite element model predicts a value of 1.2527×10^{-3} m, which is a difference of 0.3%.

Figure 20 shows a comparison of the normal stress in the x direction, σ_{xx}, for the element at the cavity surface and adjacent to the x axis for the coupled and finite element models. The value of σ_{xx} for this element is close to the value of the applied pressure at any point. (See the discussion for the previous problem.) The nonlinear behavior of the jointed rock model introduces a noticeable perturbation in the stress results in the applied pressure range of 0.3 MPa to 0.4 MPa. This perturbation, like the one for the previous problem, is probably due to the influence of slip displacements on the joint planes. Both the coupled and finite element results show this perturbation. The coupled and finite element results show close agreement over the entire applied pressure range of 0 to 0.5 MPa. At a pressure of 0. 5 MPa, the value for σ_{xx} for the cavity surface element adjacent to the x axis is -0.4506 MPa. The value for the finite element model is –0.4488 MPa, which is a difference of 0.4%.

For this second problem, the graph for u_x on the x axis at the cavity surface as a function of the applied pressure at the cavity surface for the coupled model is not as smooth as the graph for the finite element model. Near a cavity pressure of 0.4 MPa, there are several small jumps in the curve for u_x in the graph for the coupled model. This is more evident

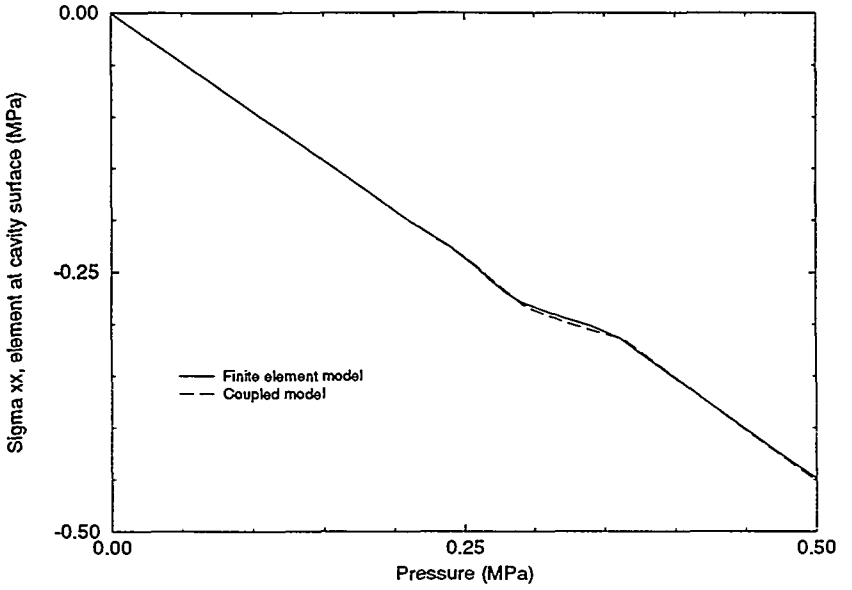

Figure 20. Comparison of Coupled and Finite Element Stress Results for an Element on the Cavity Surface (Material Interface at 27 m)

in Figure 21 where the curve for u_x for the coupled model is drawn as a solid line. Increasing the number of load increments (reducing the magnitude of the load increment for a step) will not necessarily eliminate these perturbations. Increasing the number of load increments may shift the perturbations, but they will remain in the graph for u_x somewhere near the applied pressure of 0.4 MPa, and the magnitude of the perturbations will be about the same. Some of the perturbations in the graph for u_x near the applied pressure of 0.4 MPa can be reduced by changing the scale factors used to convert the boundary element formulation from one involving nodal point tractions to one involving nodal point forces. As indicated in Reference 9, the boundary element portion of the coupled problem is formulated in terms of nodal point tractions. It is necessary to convert the nodal point tractions to nodal point forces when the boundary element model is coupled to the finite element model. Because all the elements in the boundary element contour have the same length, a single constant value converts the boundary element description of the problem from nodal point tractions to nodal point forces. For the second sample problem, the scale factor for this conversion is the arc length of the boundary element contour ($27 \times 2\pi$ m) divided by the number of elements on the boundary element contour (96). The scale factor is 0.5625π. If this number is decreased by a small amount, 1.5%, to 0.5540625π, then the graph for u_x for the point on the x axis on the cavity surface becomes slightly smoother and the agreement of the solution with the finite element results is still quite good. The graph for u_x for the reduced scale factor calculations is shown in Figure 21. When the applied

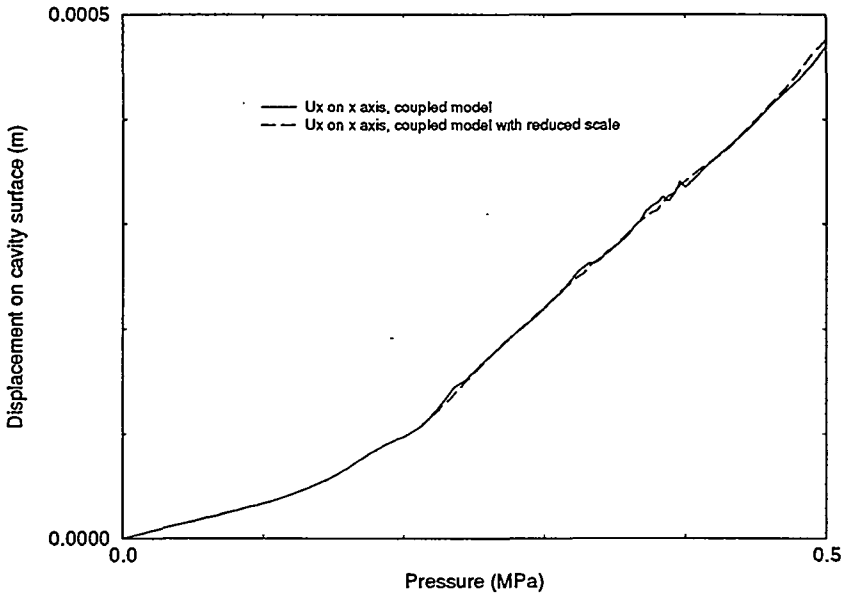

Figure 21. Results for u_x with Reduced Scale Calculations

cavity pressure is 0.5 MPa, the value for u_x for the reduced scale factor calculations is 4.7626×10^{-4} m, which varies from the finite element solution by 3.1%. At a cavity pressure of 0.5 MPa, the value for u_y at the point on the cavity surface on the y axis is 1.2548×10^{-3} m, which varies from the finite element results by 0.2%. The value for σ_{xx} for the cavity surface element adjacent to the x axis is -0.4509 MPa, which varies from the finite element results by 0.5%. The graphs for u_y and σ_{xx} are not shown. Only the results at 0.5 MPa are given here to verify that the reduced scale calculations maintain good agreement with the finite element results for these two values, u_y and σ_{xx}.

In order to do the reduced scale calculations for the second problem (r_i = 27 m), it was necessary to increase the number of load increments. For the calculations with a scale factor of 0.5625π, 340 load increments were used. To run the problem with the reduced scale factor of 0.5540625π, it was necessary to increase the number of load increments. For the solution presented in this memo, a total of 440 load increments was used.

For the first problem (r_i = 16 m), there is no incentive to try some scheme for improving the smoothness of the graphs for displacements. The graphs for u_x and u_y shown in Figure

16 for the coupled calculations show a degree of smoothness comparable to the finite element calculations. Some experimentation was done with this problem, however, to study the effects of varying the scale factor. The scale factor based on the geometry of the problem that converts the nodal point tractions to nodal point forces is the arc length of the boundary element contour ($16 \times 2\pi$ m) divided by 96, the number of elements on the contour. This gives a scale factor of $\pi/3$. The scale factor was increased by approximately 1.5% to $\pi/(2.95)$. When the cavity pressure is 1.0 MPa, the value for u_x at the point on the cavity surface on the x axis is 9.6929×10^{-4} m, which varies from the finite element results by 2.2%. The value for u_y at the point on the cavity surface on the y axis is 1.6053×10^{-3} m, which varies from the finite element results by 3.6%. Finally, the value for σ_{xx} for the cavity surface element adjacent to the x axis is -0.93914 MPa, which varies from the finite element results by 0.6%. The differences between the increased scale results and the finite element results is comparable to the differences between the results with a scale factor of $\pi/3$ and the finite element results.

Changing the scale affected not only the smoothness of the solution, but also the number of load increments required to obtain a solution. The increased scale results were obtained by using a total of 300 load increments. In order to obtain results using a scale factor of $\pi/3$, it was necessary to increase the number of load increments. The results presented in this memo with a scale factor of $\pi/3$ are for 350 load increments.

Conclusions

This report summarizes preliminary work to extend the scheme for coupling finite element and boundary element methods presented in Reference 9 from problems involving only elastic materials to problems involving nonlinear materials. The original coupling studies with strictly elastic problems required only the Bi-CGSTAB method to solve the resulting set of nonsymmetric equations. When the transition was made to coupled models involving nonlinear materials, it became necessary to use the Bi-CGSTAB approach in conjunction with a Newton solution scheme. For problems with nonlinear material behavior, it is necessary to apply the load incrementally. The Newton scheme subdivides a load increment into a series of linear problems. For each Newton iteration, the Bi-CGSTAB is used to calculate the corresponding displacement increment. The total displacement increment corresponding to the load increment is the sum of the displacement increments for each Newton iteration. This solution approach appears to be reasonably robust and accurate for the coupled problems involving nonlinear material behavior.

Since the coupled problems presented in this report involve nonlinear material behavior, it is difficult to find analytic solutions for comparison. A combination of finite element results and some limited analytic results have been used as a basis for verification. The results presented in this report indicate that the coupled scheme is producing accurate

results for problems involving elastic-plastic material behavior and jointed rock behavior. Some of the results show a high degree of accuracy. The results indicate that the coupled scheme should be quite accurate, in general, for problems where there is a nonlinear material region surrounded by a region that can be modeled reasonably well by elastic material behavior.

No timing studies have been done so far. The implementation used for these studies is experimental and certain portions of the code have not been optimized, which would make it difficult to run meaningful timing experiments. The primary objective of these initial studies has been to establish the accuracy and robustness of the coupled scheme. The question of efficiency is important primarily in regard to three-dimensional problems. The coupled scheme proposed in this report does eliminate the problem of large storage requirements, which is highly desirable. For coupled three-dimensional problems, it is probably wise to consider a simple geometry for the finite element/boundary element interface as a means of achieving an efficient coupling scheme. For the problem of a finite element region capturing nonlinear material behavior that is completely surrounded by a boundary element region, we can consider such simple shapes for the boundary element region as a parallelepiped or a sphere. These two shapes allow us to exploit symmetry, and they may also lead to simplifications in the boundary element formulation that can simplify the boundary element calculations. Simple geometric shapes may also allow the storage of boundary element information in a very compact form. Under these conditions, the boundary element information would not have to be regenerated. The advantages of limiting the finite element/boundary element interface to a simple shape is an area that needs further investigation.

In conclusion, the research presented in this report shows that an iterative solution scheme for coupled finite element/boundary element materials is a viable scheme for problems with nonlinear material behavior in the finite element region.

References

[1]Zienkiewicz, O. C., D. W. Kelly, and P. Bettess, "The Coupling of the Finite Element Method and Boundary Solution Procedures," *International Journal for Numerical Methods in Engineering*, Vol. 11, pp. 355-375, 1977. (NNA.930330.0004)

[2]Mustoe, G. G. W., F. Volait, and O. C. Zienkiewicz, "A Symmetric Direct Boundary Integral Equation Method for Two-Dimensional Elastostatics," *Res Mechanica*, Vol. 4, pp. 57-82, 1982. (NNA.930330.0018)

[3]Beer, G., "Finite Element, Boundary Element and Coupled Analysis of Unbounded Problems in Elastostatics," *International Journal for Numerical Methods in Engineering*, Vol. 19, pp. 567-580, 1983. (NNA.930330.0005)

[4]Beer, G., and G. Swoboda, "On the Efficient Analysis of Shallow Tunnels," *Computers and Geotechnics*, Vol. 1, pp. 15-31, 1985. (NNA.930330.0086)

[5]Li, H-B., G-M. Han, H. A. Mang, and P. Torzicky, "A New Method for the Coupling of Finite Element and Boundary Element Discretized Subdomains of Elastic Bodies," *Computer Methods in Applied Mechanics and Engineering*, Vol. 54, pp. 161-185, 1986. (NNA.930330.0019)

[6]Lorig, L. J., B. H. G. Brady, and P. A. Cundall, "Hybrid Distinct Element-Boundary Element Analysis of Jointed Rock," *International Journal of Rock Mechanics and Mining Sciences & Geomechanics Abstracts*, Vol. 23, No. 4, pp. 303-312, 1986. (NNA.930330.0006)

[7]Stern, M., and L. M. Taylor, *A Coupled Boundary Integral and Finite Element Formulation for Nonlinear Half-space Problems*, SAND86-1902, Sandia National Laboratories, Albuquerque, NM, 1986. (NNA.900129.0543)

[8]Subel, N., S. K. Saxena, and J. Mohammadi, "A BEM-FEM Approach for Analysis of Distresses in Pavements," *International Journal for Numerical and Analytical Methods in Geomechanics*, Vol. 15, No. 2, pp. 103-119, 1991. (NNA.930330.0007)

[9]Koteras, J. R., *Use of an Iterative Solution Method for Coupled Finite Element and Boundary Element Modeling*, SAND92-2762, Sandia National Laboratories, Albuquerque, NM, July 1993. (NNA.930701.0053)

[10]Biffle, J. H., and M. L. Blanford, *JAC2D--A Two-Dimensional Finite Element Computer Program for the Nonlinear Quasi-Static Response of Solids with the Conjugate Gradient Method*, SAND93-1891, Sandia National Laboratories, Albuquerque, NM, May 1994. (NNA.940126.0190)

[11]Kachanov, L. M., *Foundations of the Theory of Plasticity*, 2nd ed., American Elsevier Publishing Company, Inc., New York, pp. 118-121, 1971.

[12]Van der Vorst, H. A., 1992, "Bi-CGSTAB: A Fast and Smoothly Converging Variant of BI-CG for the Solution of Nonsymmetric Linear Systems," *SIAM Journal on Scientific and Statistical Computing*, Vol. 13, No. 2, pp. 631-644, March 1992. (NNA.930614.0258)

[13]Zienkiewicz, O. C., *The Finite Element Method, Third Edition*, McGraw-Hill Book Company, San Francisco, CA, 1977.

[14]Daniel, J. W., "The Conjugate Gradient Method for Linear and Nonlinear Operator Equations," *SIAM Journal of Numerical Analysis*, Vol. 4, No. 1, pp. 10-26, 1967. (NNA.920610.0031)

[15]Bartels, R., and J. W. Daniel, "A Conjugate Gradient Approach to Nonlinear Elliptic Boundary Value Problems in Irregular Regions," *Lecture Notes in Mathematics*, Edited by A. Dold and B. Eckmann, Springer-Verlag, New York, pp. 1-11, 1973. (NNA.920811.0122)

[16]Chen, E. P., *A Computational Model for Jointed Media with Orthogonal Sets of Joints*, SAND86-1122, Sandia National Laboratories, Albuquerque, NM, March 1987. (NNA.891020.0180)

[17]Koteras, J. R., *Studies of Computational Models for Jointed Media with Orthogonal Sets of Joints*, SAND89-0011, Sandia National Laboratories, Albuquerque, NM, March 1990. (NNA.900205.0069)

[18]Koteras, J. R., *An Analysis of a Joint Shear Model for Jointed Media with Orthogonal Joint Sets*, SAND89-2607, Sandia National Laboratories, Albuquerque, NM, October 1991. (NNA.900220.0012)

[19]Bauer, S. J., and L. S. Costin, *Thermal and Mechanical Codes First Benchmark Exercise Part II: Elastic Analysis*, SAND89-0757, Sandia National Laboratories, Albuquerque, NM, June 1990. (NNA.900515.0143)

[20]Costin, L. S., and S. J. Bauer, *Yucca Mountain Project Thermal and Mechanical Codes First Benchmark Exercise Part III: Jointed Rock Mass Analysis*, SAND89-1639, Sandia National Laboratories, Albuquerque, NM, October, 1991.

blank page
(do not print)

YUCCA MOUNTAIN SITE CHARACTERIZATION PROJECT

UC814 - DISTRIBUTION LIST

1 D. A. Dreyfus (RW-1)
Director
OCRWM
US Department of Energy
1000 Independence Avenue SW
Washington, DC 20585

1 L. H. Barrett (RW-2)
Acting Deputy Director
OCRWM
US Department of Energy
1000 Independence Avenue SW
Washington, DC 20585

1 S. Rousso (RW-40)
Office of Storage and Transportation
OCRWM
US Department of Energy
1000 Independence Avenue SW
Washington, DC 20585

1 R. A. Milner (RW-30)
Office of Program Management
and Integration
OCRWM
US Department of Energy
1000 Independence Avenue SW
Washington, DC 20585

1 D. R. Elle, Director
Environmental Protection Division
DOE Nevada Field Office
US Department of Energy
P.O. Box 98518
Las Vegas, NV 89193-8518

1 T. Wood (RW-14)
Contract Management Division
OCRWM
US Department of Energy
1000 Independence Avenue SW
Washington, DC 20585

4 Victoria F. Reich, Librarian
Nuclear Waste Technical Review Board
1100 Wilson Blvd., Suite 910
Arlington, VA 22209

5 Wesley Barnes, Project Manager
Yucca Mountain Site Characterization
Office
US Department of Energy
P.O. Box 98608--MS 523
Las Vegas, NV 89193-8608

1 Director
Office of Public Affairs
DOE Nevada Operations Office
US Department of Energy
P.O. Box 98518
Las Vegas, NV 89193-8518

8 Technical Information Officer
DOE Nevada Operations Office
US Department of Energy
P.O. Box 98518
Las Vegas, NV 89193-8518

1 P. K. Fitzsimmons, Technical Advisor
Office of Assistant Manager for
Environmental Safety and Health
DOE Nevada Operations Office
US Department of Energy
P.O. Box 98518
Las Vegas, NV 89193-8518

1 J. A. Blink
Deputy Project Leader
Lawrence Livermore National Laboratory
101 Convention Center Drive
Suite 820, MS 527
Las Vegas, NV 89109

2 J. A. Canepa
Technical Project Officer - YMP
N-5, Mail Stop J521
Los Alamos National Laboratory
P.O. Box 1663
Los Alamos, NM 87545

1 Repository Licensing & Quality
Assurance
Project Directorate
Division of Waste Management
US NRC
Washington, DC 20555

1 Senior Project Manager for Yucca
Mountain
Repository Project Branch
Division of Waste Management
US NRC
Washington, DC 20555

1 NRC Document Control Desk
Division of Waste Management
US NRC
Washington, DC 20555

1 Chad Glenn
NRC Site Representative
301 E Stewart Avenue, Room 203
Las Vegas, NV 89101

1 E. P. Binnall
Field Systems Group Leader
Building 50B/4235
Lawrence Berkeley Laboratory
Berkeley, CA 94720

1 Center for Nuclear Waste
Regulatory Analyses
6220 Culebra Road
Drawer 28510
San Antonio, TX 78284

2 W. L. Clarke
Technical Project Officer - YMP
Attn: YMP/LRC
Lawrence Livermore National Laboratory
P.O. Box 5514
Livermore, CA 94551

1 V. R. Schneider
Asst. Chief Hydrologist -- MS 414
Office of Program Coordination
and Technical Support
US Geological Survey
12201 Sunrise Valley Drive
Reston, VA 22092

1 J. S. Stuckless, Chief
Geologic Studies Program
MS 425
Yucca Mountain Project Branch
US Geological Survey
P.O. Box 25046
Denver, CO 80225

1 N. Z. Elkins
Deputy Technical Project Officer
Los Alamos National Laboratory
Mail Stop 527
101 Convention Center Drive, #820
Las Vegas, NV 89109

2 Michaele C. Brady
Technical Project Officer - YMP
Sandia National Laboratories
Organization 6302, MS 1399
101 Convention Center Drive, Suite 880
Las Vegas, NV 89109

1 Ray Wallace
US Geological Survey
106 National Center
12201 Sunrise Valley Drive
Reston, VA 22092

1 L. R. Hayes
Technical Project Officer
Yucca Mountain Project Branch
MS 425
US Geological Survey
P.O. Box 25046
Denver, CO 80225

1 A. L. Flint
US Geological Survey
MS 721
P.O. Box 327
Mercury, NV 89023

1 R. E. Lewis
Yucca Mountain Project Branch
MS 425
US Geological Survey
P.O. Box 25046
Denver, CO 80225

1 D. Zesiger
US Geological Survey
101 Convention Center Drive
Suite 860, MS 509
Las Vegas, NV 89109

2 L. D. Foust
Nevada Site Manager
TRW Environmental Safety Systems
101 Convention Center Drive
Suite P-110, MS 423
Las Vegas, NV 89109

1 C. E. Ezra
YMP Support Office Manager
EG&G Energy Measurements Inc.
MS V-02
P.O. Box 1912
Las Vegas, NV 89125

1 E. L. Snow, Program Manager
Roy F. Weston, Inc.
955 L'Enfant Plaza SW
Washington, DC 20024

1 Technical Information Center
Roy F. Weston, Inc.
955 L'Enfant Plaza SW
Washington, DC 20024

1 Technical Project Officer - YMP
US Bureau of Reclamation
Code D-3790
P.O. Box 25007
Denver, CO 80225

1 B. T. Brady
Records Specialist
US Geological Survey
MS 421
P.O. Box 25046
Denver, CO 80225

1 M. D. Voegele
Technical Project Officer - YMP
M&O/SAIC
101 Convention Center Drive
Suite 407
Las Vegas, NV 89109

1 Paul Eslinger, Manager
PASS Program
Pacific Northwest Laboratories
P.O. Box 999
Richland, WA 99352

1 A. T. Tamura
Science and Technology Division
OSTI
US Department of Energy
P.O. Box 62
Oak Ridge, TN 37831

1 P. J. Weeden, Acting Director
Nuclear Radiation Assessment Div.
US EPA
Environmental Monitoring Sys. Lab
P.O. Box 93478
Las Vegas, NV 89193-3478

1 ONWI Library
Battelle Columbus Laboratory
Office of Nuclear Waste Isolation
505 King Avenue
Columbus, OH 43201

1 C. H. Johnson
Technical Program Manager
Agency for Nuclear Projects
State of Nevada
Evergreen Center, Suite 252
1802 N. Carson Street
Carson City, NV 89710

1 John Fordham, Deputy Director
Water Resources Center
Desert Research Institute
P.O. Box 60220
Reno, NV 89506

1 The Honorable Cyril Schank
Chairman
Churchill County Board of
Commissioners
190 W. First Street
Fallon, NV 89406

1 T. Hay, Executive Assistant
Office of the Governor
State of Nevada
Capitol Complex
Carson City, NV 89710

3 R. R. Loux
Executive Director
Agency for Nuclear Projects
State of Nevada
Evergreen Center, Suite 252
1802 N. Carson Street
Carson City, NV 89710

1 Brad R. Mettam
Inyo County Yucca Mountain
Repository Assessment Office
P. O. Drawer L
Independence, CA 93526

1 Lander County Board of Commissioners
315 South Humbolt Street
Battle Mountain, NV 89820

1 Vernon E. Poe
Office of Nuclear Projects
Mineral County
P.O. Box 1600
Hawthorne, NV 89415

1 Les W. Bradshaw
Program Manager
Nye County Nuclear Waste Repository
Project Office
P.O. Box 1767
Tonopah, NV 89049

1 Florindo Mariani
White Pine County Coordinator
P. O. Box 135
Ely, NV 89301

1 Judy Foremaster
City of Caliente Nuclear Waste
Project Office
P.O. Box 158
Caliente, NV 89008

1 Philip A. Niedzielski-Eichner
Nye County Nuclear Waste
Repository Project Office
P.O. Box 221274
Chantilly, VA 22022-1274

1 Dennis Bechtel, Coordinator
Nuclear Waste Division
Clark County Department of
Comprehensive Planning
301 E. Clark Avenue, Suite 570
Las Vegas, NV 89101

1 Juanita D. Hoffman
Nuclear Waste Repository
Oversight Program
Esmeralda County
P.O. Box 490
Goldfield, NV 89013

1 Eureka County Board of Commissioners
Yucca Mountain Information Office
P.O. Box 714
Eureka, NV 89316

1 Economic Development Dept.
City of Las Vegas
400 E. Stewart Avenue
Las Vegas, NV 89101

1 Community Planning & Development
City of North Las Vegas
P.O. Box 4086
North Las Vegas, NV 89030

1 Community Development & Planning
City of Boulder City
P.O. Box 61350
Boulder City, NV 89006

1 Commission of European Communities
200 Rue de la Loi
B-1049 Brussels
BELGIUM

2 Librarian
YMP Research & Study Center
MS 407
P.O. Box 98521
Las Vegas, NV 89193-8521

1 Amy Anderson
Argonne National Laboratory
Building 362
9700 S. Cass Avenue
Argonne, IL 60439

1 Glenn Van Roekel
Director of Community Development
City of Caliente
P.O. Box 158
Caliente, NV 89008

1 G. S. Bodvarsson
Head, Nuclear Waste Department
Lawrence Berkeley Laboratory
1 Cyclotron Road, MS 50E
Berkeley, CA 94720

1 Michael L. Baughman
Intertech Services Corp.
P.O. Box 93537
Las Vegas, NV 89193

	MS	
2	1330	C. B. Michaels, 6752 100/1.2.4.2.3.1 SAND95-2081/QA
20	1330	WMT Library, 6752
10	0443	J. R. Koteras, 1517
1	0443	H. S. Morgan, 1517
1	0841	P. J. Hommert, 1500
1	0827	R. D. Skocypec, 1502
1	0841	J. H. Biffle, 1503
1	0437	R. K. Thomas, 1518
1	0439	D. R. Martinez, 1434
1	9018	Central Technical Files, 8523-2
5	0899	Technical Library, 4414
1	0619	Print Media, 12615
2	0100	Document Processing, 7613-2 for DOE/OSTI